Overview of the inorganic and organic composition of size-segregated aerosol in Rondônia, Brazil, from the biomass-burning period to the onset of the wet season

Sandro Fuzzi,[1] Stefano Decesari,[1] Maria Cristina Facchini,[1] Fabrizia Cavalli,[1]
Lorenza Emblico,[1] Mihaiela Mircea,[1] Meinrat O. Andreae,[2] Ivonne Trebs,[2]
András Hoffer,[2] Pascal Guyon,[2] Paulo Artaxo,[3] Luciana V. Rizzo,[3]
Luciene L. Lara,[3] Theotonio Pauliquevis,[3] Willy Maenhaut,[4] Nico Raes,[4]
Xuguang Chi,[4] Olga L. Mayol-Bracero,[5] Lydia L. Soto-García,[5] Magda Claeys,[6]
Ivan Kourtchev,[6] Jenny Rissler,[7] Erik Swietlicki,[7] Emilio Tagliavini,[8,9] Gal Schkolnik,[10]
Alla H. Falkovich,[10] Yinon Rudich,[10] Gilberto Fisch,[11] and Luciana V. Gatti[12]

[1]   The aerosol characterization experiment performed within the Large-Scale Biosphere-Atmosphere Experiment in Amazonia–Smoke, Aerosols, Clouds, Rainfall and Climate (LBA-SMOCC) field experiment carried out in Rondônia, Brazil, in the period from September to November 2002 provides a unique data set of size-resolved chemical composition of boundary layer aerosol over the Amazon Basin from the intense biomass-burning period to the onset of the wet season. Three main periods were clearly distinguished on the basis of the PM_{10} concentration trend during the experiment: (1) dry period, with average PM_{10} well above 50 $\mu g\ m^{-3}$; (2) transition period, during which the 24-hour-averaged PM_{10} never exceeded 40 $\mu g\ m^{-3}$ and never dropped below 10 $\mu g\ m^{-3}$; (3) and wet period, characterized by 48-hour-averaged concentrations of PM_{10} below 12 $\mu g\ m^{-3}$ and sometimes as low as 2 $\mu g\ m^{-3}$. The trend of PM_{10} reflects that of CO concentration and can be directly linked to the decreasing intensity of the biomass-burning activities from September through November, because of the progressive onset of the wet season. Two prominent aerosol modes, in the submicron and supermicron size ranges, were detected throughout the experiment. Dry period size distributions are dominated by the fine mode, while the fine and coarse modes show almost the same concentrations during the wet period. The supermicron fraction of the aerosol is composed mainly of primary particles of crustal or biological origin, whereas submicron particles are produced in high concentrations only during the biomass-burning periods and are mainly composed of organic material, mostly water-soluble, and ∼10% of soluble inorganic salts, with sulphate as the major anion. Size-resolved average aerosol chemical compositions are reported for the dry, transition, and wet periods. However, significant variations in the aerosol composition and concentrations were observed within each period, which can be classified into two categories: (1) diurnal oscillations, caused by the diurnal cycle of the boundary layer and the different combustion phase active during day (flaming) or night (smouldering); and (2) day-to-day variations, due to alternating phases of relatively wet and dry conditions. In a second part of the study, three subperiods representative of the

[1]Institute of Atmospheric Sciences and Climate, National Research Council, Bologna, Italy.

[2]Biogeochemistry Department, Max Planck Institute for Chemistry, Mainz, Germany.

[3]Instituto de Fisica, Universidade de São Paulo, São Paulo, Brazil.

[4]Department of Analytical Chemistry, Institute for Nuclear Sciences, Ghent University, Ghent, Belgium.

[5]Institute for Tropical Ecosystem Studies, University of Puerto Rico, San Juan, Puerto Rico, USA.

[6]Department of Pharmaceutical Sciences, University of Antwerp, Antwerp, Belgium.

[7]Division of Nuclear Physics, Department of Physics, Lund University, Lund, Sweden.

[8]Dipartimento di Chimica "G. Ciamician", University of Bologna, Bologna, Italy.

[9]Also at Centro di Ricerche per le Scienze Ambientali, University of Bologna, Ravenna, Italy.

[10]Department of Environmental Sciences, Weizmann Institute, Rehovot, Israel.

[11]Centro Técnico Aeroespacial, Instituto de Aeronáutica e Espaço, Divisão de Ciências Atmosféricas, São José dos Campos, São Paulo, Brazil.

[12]Divisao de Quimica Ambiental, Instituto de Pesquisas Energéticas e Nucleares, São Paulo, Brazil.

conditions occurring in the dry, transition, and wet periods were isolated to follow the evolution of the aerosol chemical composition as a function of changes in rainfall rate and in the strength of the sources of particulate matter. The chemical data set provided by the SMOCC field experiment will be useful to characterize the aerosol hygroscopic properties and the ability of the particles to act as cloud condensation nuclei.
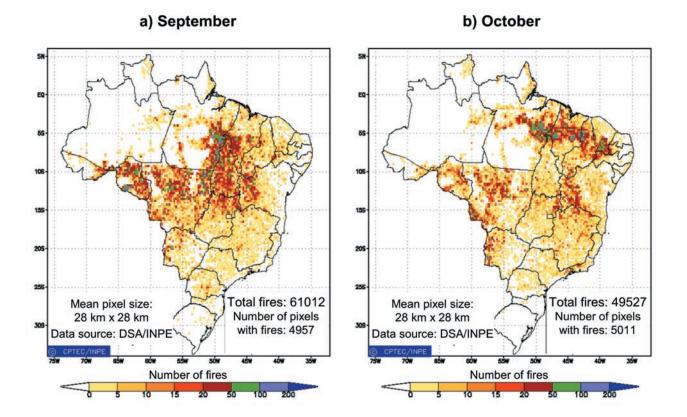
1. Introduction

[2] The Large-Scale Biosphere-Atmosphere Experiment in Amazonia–Smoke, Aerosols, Clouds, Rainfall and Climate (LBA-SMOCC) field campaign was conducted in Rondônia, southwest of Amazonia, Brazil, in the period from September to November 2002, extending from the intense biomass-burning period to the onset of the wet season. The overall goal of SMOCC was to investigate the connection between the physical and chemical properties and the abundance of biomass-burning aerosol particles, with changes in cloud microphysical properties, such as the decreasing of the size of cloud droplets forming on this aerosol, and the climatic consequences of the resulting perturbation of cloud physics [*Andreae et al.*, 2004]. For this purpose, a full physical and chemical characterization of the aerosol particles throughout the experimental period was carried out, in order to determine the link between the aerosol chemical and physical properties and their hygroscopic and cloud-nucleating properties. The data obtained will also provide input for models simulating the effect of biomass-burning aerosol on cloud microphysics [*Roberts et al.*, 2002], with the aim of investigating the effect of smoke aerosols on climate dynamics and the resulting large-scale climatic effects. Aerosols emitted during biomass burning are predominantly in the form of submicrometer, accumulation-mode particles [*Artaxo et al.*, 2002]. While the inorganic composition of this aerosol and its emission factors from fires have been determined in a number of previous studies [*Artaxo et al.*, 1998, 2000, 2002; *Andreae et al.*, 1998; *Reid et al.*, 1998; *Formenti et al.*, 2003], there is still very little information about its organic composition, although organic matter is known to constitute the major fraction of smoke aerosols, accounting for up to 80% of the total aerosol mass [*Artaxo and Hansson*, 1995]. The organic material within smoke aerosols is composed of a highly complex mixture of compounds, covering a wide range of molecular structures, physical properties and reactivities. Apart from a few field studies that have shown that water-soluble organic acids are significantly enriched in smoke aerosol [*Mayol-Bracero et al.*, 2002; *Gao et al.*, 2003], very little work has gone into the sampling of fresh and aged biomass smoke to determine the quantity and molecular forms of the oxygenated, water-soluble organic compounds (WSOC) produced by biomass burning. The need for the analysis of this fraction, however, has gained in relevance since it has now been shown that the burning of cellulose produces smoke particles that are nearly 100% water-soluble [*Novakov and Corrigan*, 1996], in addition to mounting evidence that water-soluble organics significantly contribute to the cloud condensation nuclei (CCN) activity of aerosols [*Roberts et al.*, 2002]. Moreover, the high concentrations of WSOC within smoke aerosols suggest that they may play a significant role in the aqueous phase chemistry occurring within cloud droplets nucleated by smoke [*Herrmann*, 2003]. Thus for the LBA-SMOCC project additional and novel methods for the analysis of organic aerosols were developed and applied [*Decesari et al.*, 2006].

[3] The purpose of this paper is to provide an overview of the LBA-SMOCC experiment itself, and describe measurements of the size segregated aerosol composition during the whole field campaign. After this overall description, some characteristic periods within the campaign are analysed and discussed in greater detail to provide deeper insight on the evolution of size-segregated aerosol composition from the dry (burning) season to the onset of the wet season.

2. Experimental Part

[4] The ground-based part of the LBA-SMOCC field experiment was performed at the Fazenda Nossa Senhora Aparecida (FNS) (10°04.70s, 61°56.02′W, 145 m asl.), a rural site in central Rondônia. The ground-based component was complemented by a large-scale airborne experiment aimed at looking at vertical profiles and measuring large-scale aerosol and cloud properties [*Andreae et al.*, 2004]. The field site was deforested by fire about 25 years ago and is now a pasture, with *Brachiaria brizantha* as the dominant species of grass. A complete description of the site as well as maps at different scales is given by *Andreae et al.* [2002]. The period of the experiment encompasses the late dry season (September to early October) and extends to the onset of the rainy period in this part of Amazonia (November). In 2002, the weather typical of the dry season lasted until the first week of October, while the rest of that month was a transition period characterized by intermittent precipitation episodes and dry days (M. A. F. Silva Dias, in preparation, 2006). During the dry season and, to a lesser extent, the transition period, widespread fire activity was observed in Rondônia and Mato Grosso, as well as in the other states that contain the "arc of deforestation" along the southern and south eastern margin of the Amazon forest (Figures 1a–1c). During the SMOCC campaign, the most intense nearby burning was taking place at the edge of the woodlands, extending from north to east of the FNS site at a distance of about 20–30 km. Wood burning was also active in Ouro Preto de Oeste (~40,800 inhabitants) which is 8 km from the sampling site. The FNS site is located on a strip of cleared land 4 km wide and several tens of kilometers long, where only sparse domestic fires were observed. Biomass burning was substantially reduced in the region at the beginning of November after the onset of persistent wet conditions.
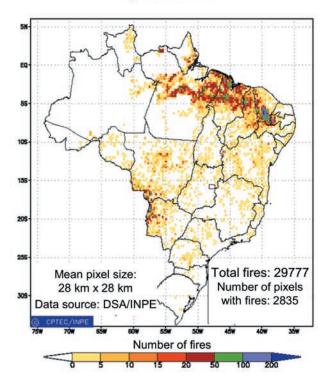
Figure 1. Monthly cumulated number of fire points over Brazil detected by the NOAA-12 satellite during the period of the SMOCC campaign: (a) September, (b) October, and (c) November 2002. Courtesy of Centro de Previsão de Tempo e Estudios Climaticos, Instituto Nacional de Pesquisas Espaciais (CPTEC/INPE).

2.1. Overview of the Meteorological Situation

[5] From the climatological records of the dry-to-wet season transition in Rondônia [*Ferreira da Costa et al.*, 1998], the average rainfall amount varies from a monthly total of 96 mm (with 6 days of rainfall higher than 1 mm/day) in September, to 153 mm (with 12 days of rainfall) in October, up to 238 mm (with 16 days of rainfall) in November. The air temperature is less variable during the period considered, with monthly mean values around 25.0°C, although there is a variation in the daily maximum temperature span: 10.7°C in September, 9.4°C in October and 8.0°C in November. This is due to the increase of minimum temperature and a slight decrease in the maximum temperature.

[6] The weather conditions during the LBA-SMOCC experiment were mainly consistent with the above climatology: temperatures were around the average (deviations less than 1°C from the average) throughout the period, with the rainfall slightly above normal in September (deviation of up to 50 mm) and November (25 mm up to 100 mm) and slightly below average in October (up to −50 mm). Radiosoundings were performed at the sampling site in order to identify the vertical structure and characteristics of the convective boundary layer (CBL) (G. Fisch, in preparation, 2006). The soundings were performed several times per day (08, 11, 14 and 17 Local Time (LT)) and the 17 LT soundings were used to represent the maximum height of the CBL. During the dry season, the boundary layer was very well mixed and developed, with an average height of around 1690 m (standard deviation. 250 m) at midday. For the transition period, when some systematic convective rainfalls developed during the afternoons, the CBL average height was reduced to around 1320 m (standard deviation. 250 m). The nocturnal boundary layer height was much lower, with maximum height approximately 200–250 m. The surface cooling due to the nocturnal radiation budget is the main force for the developing of this layer as winds are very weak. No soundings are available for the last period of the campaign, i.e., after 31 October at the onset of the wet season. The evolution of the boundary layer is also discussed in a paper by *Rissler et al.* [2006].

2.2. Aerosol Sampling and Analysis

[7] The experimental set-up employed during the LBA-SMOCC campaign at the FNS site was designed for a full characterization of the optical, physical, hygroscopic and chemical properties of the aerosol [*Chand et al.*, 2006; *Decesari et al.*, 2006; *Trebs et al.*, 2005, 2006]. Trace gas (CO and NO_x) concentrations were also measured throughout the experiment. CO was measured with the Thermo Environmental Instrument Inc. analyzer (Model 48C Gas Filter Correlation) with a detection limit of 40 ppb. Because of the high ambient humidity, a cooler was used to remove water from the sample stream prior to the CO analyzer. The chemiluminescence NO/NO_x analyzer (Model 42C TL, Thermo Environment Instruments Inc.) was equipped with a molybdenum converter to transform ambient NO_2 to NO (for details, see *Trebs et al.* [2006]). The dry aerosol number size distributions were measured with a Differential Mobility Particle Sizer (DMPS) at a time resolution of 10 min [*Rissler et al.*, 2004]. The aerosol entered the DMPS at ambient relative humidity. The DMPS was operated in stepping mode, measuring at steps of equal logarithmic diameter, for a total of 38 mobility channels covering the size range from 3 to 850 nm. The inversion program converting the measured mobility distribution to dry number size distributions takes into account sampling line losses, bipolar charging probabilities, calibrated DMA transfer functions, DMA diffusion broadening and losses, and CPC counting efficiencies. PM_{10} and $PM_{2.5}$ were determined every 30 min by means of two Tapered Element Oscillating Microbalance (TEOM) instruments, operating at an inlet temperature of 50 degrees. Aerosol total carbon (TC) in $PM_{2.5}$ and its volatile and refractory fractions, were determined every 60 min with a R&P Ambient Carbon Particulate Monitor series 5400 [*Artaxo et al.*, 2002]. With the R&P 5400, refractory carbon was derived as the fraction of carbon that is converted to CO_2 above a temperature of 350°C. Organic carbon was obtained as the difference between total carbon and refractory carbon. The TEOMs and the carbon monitor were operated at the FNS site throughout the campaign until 3 November.

[8] A combination of wet annular denuder/steam jet aerosol collector (SJAC) was used to measure the concentrations of inorganic aerosol species (ammonium, nitrate, nitrite, chloride and sulphate) and their gaseous precursors (ammonia, nitric acid, nitrous acid, hydrochloric acid and sulphur dioxide) online with a time resolution of 20 min from 12 to 23 September, and of 40–60 min from 7 October to 11 November [*Trebs et al.*, 2004].

[9] Aerosol samples for chemical analysis were collected by means of a suite of filter samplers and five different models of cascade impactors. The characteristics of the impactors are reported in Table 1. The filter samplers included PM_{10} and $PM_{2.5}$ collectors, stacked filter unit (SFU) samplers, and high-volume dichotomous samplers (HVDS). The SFU samplers and HVDS provide separate coarse and fine size fractions, with coarse being the size range 2–10 μm aerodynamic diameter (AD) for the SFU and >2.5 μm AD for the HVDS, and fine being the size range of <2 μm AD for the SFU and <2.5 μm AD for the HVDS. The chemical analyses for the filter samples are described elsewhere [*Falkovich et al.*, 2005; *Decesari et al.*, 2006; W. Maenhaut, in preparation, 2006; M. Claeys, in preparation, 2006]. Among the techniques for measuring individual chemical species or elements in the filter samples were ion chromatography (IC), gas chromatography/mass spectrometry (GC/MS), instrumental neutron activation analysis (INAA) and particle-induced X-ray emission spectrometry (PIXE). The sampling time for all aerosol collection devices was initially set at 12 hours, and then extended to 24 and 48 hours following the decrease in the aerosol air concentrations monitored by TEOM. The collectors were operated in parallel with the exception of the 8-stage micro-orifice uniform deposition impactor (MOUDI). Because of expected differences in the concentrations and composition of the aerosol during day and night [*Artaxo et al.*, 2002], samplings were performed separately for day and night conditions. Therefore during the transition and wet periods, 24 and 48 hour diurnal/nocturnal samplings were performed on two and four consecutive days/nights, respectively.

[10] The 13-stage Dekati low-pressure impactor (DLPI), 11-stage MOUDI and the 5-stage Berner Impactor (BI) used aluminium foils for the determination of particulate mass

Table 1. Cascade Impactors Deployed During the SMOCC Field Experiment by the Various Groups Participating in the Field Experiment[a]

Impactor Type	Dekati Low-Pressure Impactor DLPI	MOUDI (Micro-orifice Uniform Deposit Impactor)		Berner Low-Pressure Impactor LPI 80	Small Deposit Area Low-Pressure Impactor (SDI)
Operator	UPR	UGent	IFUSP	ISAC	UGent
Sampling period	15 Sept to 14 Nov	9 Sept to 14 Nov	15 Sept to 14 Nov	8–28 Sept; 15 Oct to 9 Nov.	9 Sept to 14 Nov
Flow rate (Lpm)	28.9–28.3	27	20–25	80[b]	11
Lower cut off (μm)	0.030[c]	0.053	0.09	0.05	0.045
	0.079[c]	0.094	0.18	0.14	0.086
	0.104[c]	0.164	0.33	0.42	0.153
	0.162	0.301	0.56	1.2	0.231
	0.269	0.603	1.00	3.5	0.343
	0.393	1.0	1.80		0.591
	0.628	1.8	3.20		0.796
	0.970	3.1	10.0		1.06
	1.64	6.2			1.66
	2.44	9.9			2.68
	4.09	18			4.08
	6.73				8.5
	10.2				
Inlet cut-size (μm)	30	None	30	10	15
Substrates	Aluminum or quartz fiber filters	Aluminum	Polycarbonate	Aluminum[g] and Tedlar	polycarbonate
Weighting (RH)	50%	50%	N.A.	30%	
Analysis	Gravimetry, EGA, ICP[d], IC[d]	Gravimetry; TOC[d,e], GCMS[d]	Gravimetry, IC[d], IEC[d]	on aluminum foils: gravimetry; on Tedlar foils: IC, TOC[f], IC-UV, NMR[d]	PIXE

[a]UPR: University of Puerto Rico; UGent: Ghent University; IFUSP: Instituto de Fisica, Universidade de São Paulo; ISAC: Institute of Atmospheric Sciences and Climate. The cut-offs are provided as aerodynamic diameters (AD).

[b]Nominal flow rate.

[c]Average cut-off for the experiment. The actual values vary among samplings.

[d]On selected samples.

[e]Thermal analysis of TC directly on the impactor foils.

[f]Thermal analysis of TC in the water extracts of the impactor foils.

[g]Mounted only in the sampling period 8–28 September.

(PM). Selected samples from the 11-stage MOUDI were analysed for TC with a TOC (total organic carbon) analyser with Solid Sample Module (Shimadzu) and selected DLPI samples were analysed for TC by evolved gas analysis (EGA) [*Novakov et al.*, 1997] and for inorganic and organic ionic species by IC [*Andreae et al.*, 2000; *Gabriel et al.*, 2002]. Elemental carbon (EC) was determined by EGA in the fine fraction from the HVDS, after water extraction to remove soluble inorganic and organic species to reduce the artifacts resulting from catalysis and charring [*Mayol-Bracero et al.*, 2002; *Hoffer et al.*, 2005].

[11] Quartz fiber filters and aluminium foils were alternatively mounted on the DLPI, with the quartz substrates allowing more accurate analysis of TC by EGA analysis, of inorganic ions by IC and of elements by Inductively Coupled Plasma Atomic Emission Spectrometry (ICP-AES). The BI was equipped with double aluminium/Tedlar substrates [*Matta et al.*, 2003] during the first period of sampling (9–28 September) and with only Tedlar substrates during the second period (15 October to 9 November). Tedlar substrates had been thoroughly washed with deionized water before sampling. Aerosols collected on Tedlar foils were extracted with water for the determination of total water-soluble organic compounds (WSOC) by liquid TOC analysis [*Decesari et al.*, 2006],

and of inorganic ions by IC [*Matta et al.*, 2003]. A 12-stage small deposit area low-pressure impactor (SDI) was specifically devoted to elemental analysis. Samples were collected on Kimfol polycarbonate foils and analysed by PIXE [*Maenhaut et al.*, 1996].

[12] The organic analysis was performed by means of different analytical techniques for both speciation at the molecular level and functional group analysis. A detailed description of the organic chemical characterization is given by *Decesari et al.* [2006]. Briefly, ion exchange chromatography coupled to UV detection for fractionation of WSOC into neutral and acidic compounds was performed on all BI samples collected on Tedlar substrates. IC and ion exclusion chromatography (IEC) for the analysis of inorganic ions, low molecular weight organic acids and hydroxylated compounds were performed on selected 8-stage MOUDI samples [*Falkovich et al.*, 2005; *Schkolnik et al.*, 2005]. The 11-stage MOUDI samples representative of the various periods of the campaign were also extracted with dichloromethane/methanol for GC/MS analysis of the polar fraction of organic carbon (OC) (M. Claeys, in preparation, 2006). Finally, two BI samples collected during episodes of very high aerosol concentrations were subjected to functional group analysis by proton nuclear magnetic resonance (NMR) spectroscopy [*Tagliavini et al.*, 2006]. For both

filters and impactor foils, blanks were stored in the field with an approximate frequency of one every ten samples. All data reported in the paper are corrected for blanks.

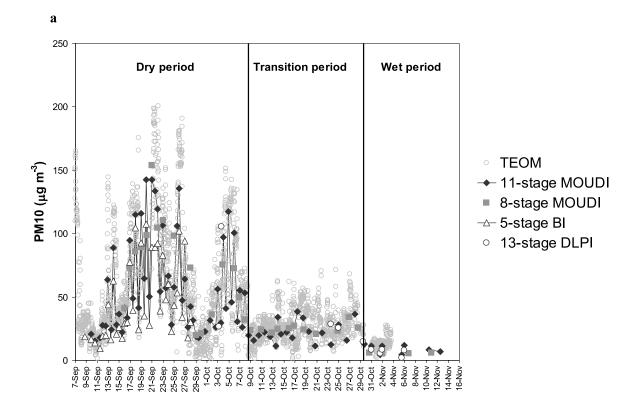## 3. Aerosol Composition and Trends

[13] The trend in ambient aerosol concentrations (PM_{10}) throughout the experiment is shown in Figure 2a. Three main periods can be clearly distinguished on the basis of the PM_{10} concentration trends: (1) dry period (from 7 September until 7 October) including two major episodes of subsequent days showing PM_{10} constantly above 50 μg m^{-3}; (2) transition period (8–30 October), 20 days during which the 24-hour-averaged PM_{10} never exceeded 40 μg m^{-3} and never dropped below 10 μg m^{-3}; (3) wet period (after 30 October) characterized by 48-hour-averaged concentrations of PM_{10} below 12 μg m^{-3} and sometimes as low as 2 μg m^{-3}. These low values of PM_{10} concentrations are characteristic of the wet season in Amazonia [*Artaxo et al.*, 2002]. The trend of PM_{10} reflects that of CO concentrations ($r^2 = 0.87$) and can be directly linked to the decreasing intensity of the biomass-burning activities from September through November due to the progressive onset of the wet season (Figure 2b). It is possible to observe that local Rondônia fires explain only part of the PM_{10} variability but, for some periods, high PM_{10} concentrations were observed with low fire counts in Rondônia. During these periods, fires in the nearby Mato Grosso state might have been responsible for the observed high PM_{10} concentrations, pointing to the importance of regional aerosol transport over Amazonia. The mean circulation was responsible for the net transport of smoke from Mato Grosso and other upwind regions to Rondônia, and from Rondônia in the south/southeastern direction, along the margin of the Andes mountains (M. A. F. Silva Dias, in preparation, 2006).

[14] The large difference in the height of the boundary layer between night and day is responsible for the oscillations in the 12-hour-averaged PM_{10} concentrations which can be observed especially during the dry period (Figure 2a), with higher ground concentrations at nighttime [*Rissler et al.*, 2006]. For example, from 17 to 20 September the aerosol concentration measured by the 11-stage MOUDI impactor varied by a factor of two between night and day, whereas the 24-hour-averaged concentrations (measured by the 8-stage MOUDI impactor) indicated only a 10% variation between consecutive samples. Because of such diurnal cycles of the aerosol concentration and to the 24-hour periodicity of other phenomena connected with the aerosol cycle (e.g., turbulence and cloud formation, biomass burning and other anthropogenic activities, biological activity), in the following sections we will discuss separately nocturnal and diurnal aerosol populations and size distributions.

[15] Despite the general agreement among the trends of PM_{10} measured by the different impactors, significant deviations were frequently observed. The integrated mass from DLPI was alternatively higher or lower than that determined by MOUDIs. Conversely, the BI provided systematically lower PM_{10} concentrations than the other three impactors (Figure 2a). The different weighting conditions employed (Table 1) may have contributed to the observed discrepancies between the impactor measurements. However, the change in the aerosol volume due to water uptake between 30 and 50% RH is estimated to be less than 10% on the basis of the measurements performed with a Hygroscopic Tandem Differential Mobility Analyzer (H-TDMA, *Rissler et al.* [2006]). The main losses of BI compared to MOUDIs were observed in different size ranges, especially above 3.5 μm and below 0.42 μm. The integrated concentrations of PM and of the chemical components determined on the BI were on average 22% lower compared to that determined on the 11-stage MOUDI, with the larger deviations observed during daytime, when the low relative humidity shifted the mode in the PM size distribution at aerosol diameters below 0.42 μm (see the following section). However, the chemical analyses showed that the same artifacts observed for PM were also found for all main chemical constituents of the aerosol, so that the ratio of individual chemical components to PM in the different size ranges was essentially the same as that found in the other impactors. Therefore we can conclude that sampling with BI was affected mostly by nonspecific artifacts with respect to the chemical composition of the aerosol particles.

3.1. Aerosol Mass and Volume Size Distributions

[16] The PM size distributions during the experiment were systematically determined by sampling with an 11-stage MOUDI (80 samples) and an 8-stage MOUDI (33 samples). Size-resolved PM data were also provided by the BI and by the DLPI, but with lower time coverage compared to the MOUDIs. Figures 3a–3c report the statistics of the measured 11-stage MOUDI size distributions for the three main periods of the campaign. Since the aerosol concentrations followed a diurnal cycle for most of the time, the average size distributions were calculated separately for the daytime and the nighttime samples. Two prominent modes, in the submicron and supermicron size ranges, respectively, were detected throughout the experiment, but the relative magnitude of the two changed according to the period. Dry period size distributions are dominated by the fine mode, but the fine and coarse modes show almost the same concentrations during the wet period. These findings are in agreement with those provided by past LBA measurement campaigns in Rondônia [*Artaxo et al.*, 2002; *Guyon et al.*, 2003], showing that the intense biomass-burning activity is reflected by high concentrations of submicron particles, whereas the pristine Amazon Basin environment is characterized by higher concentrations of coarse-mode biogenic particles emitted by the vegetation. During the LBA-SMOCC experiment, fine-mode particle concentrations decreased by a factor of 20 from the dry to the wet period, while the coarse-mode particle concentrations were relatively stable throughout the campaign, suggesting that the natural background of supermicron particles is almost constant during the dry-to-wet season transition.

[17] The average concentrations of both fine and coarse particles were lower during the day than during the night, supporting the proposed dilution effect due to the evolution of the boundary layer that is much higher during daytime, as a result of intense vertical mixing and dilution. Another distinguishing feature of daytime PM size distribution is the occurrence of two overlapping modes in the submicron fraction at ∼300 and 700 nm which correspond to the "condensation" (lower submicron) and "droplet" (upper
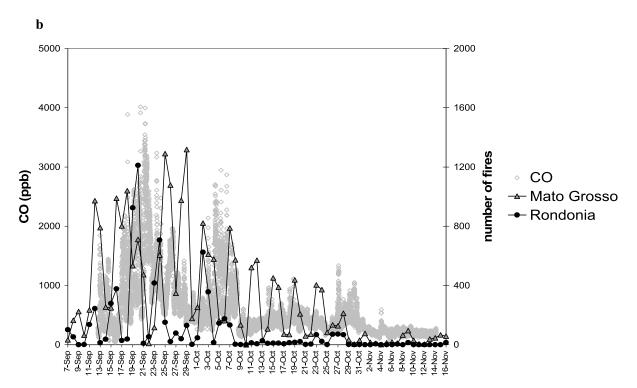
Figure 2. (a) Trends in PM_{10} concentrations from TEOM and from integrated impactor measurements versus GMT throughout the experiment. (b) Trends in CO concentrations and of fire spots versus GMT in the states of Rondônia and Mato Grosso measured by NOAA-14. The time resolution is 5 min for the CO monitor, 30 min for TEOM and 12 to 48 h for the impactors.
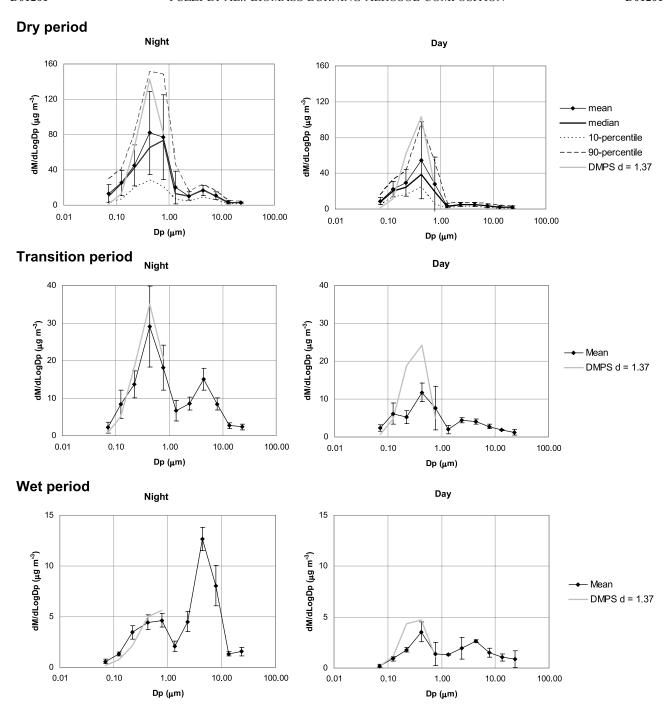
Figure 3. PM size distributions from the 11-stage MOUDI. Mass size distributions derived from integrated DMPS volume size distributions assuming a dry density of 1.37 are also reported. (a) Dry period; (b) transition period; (c) wet period. Percentiles were not calculated in the cases of transition period and wet period samples, because of the small number of samples (n ≤ 5) in each subset.

submicron) modes, respectively [*Maenhaut et al.*, 2004]. Finally, during the dry period, the mean modal diameter in the submicron size range is higher during the night than during the day, possibly because of the marked difference in relative humidity (RH) between day and night (near 50 and 100%, respectively), promoting hygroscopic growth of the aerosol during nighttime [*Trebs et al.*, 2005]. The diameter growth factors of the aerosol (between <15% and 90% RH)

measured by a hygroscopic tandem DMA (HTDMA) ranged from 1.1 to 1.3 for particles having dry diameter of 50−440 nm [*Rissler et al.*, 2006]. By taking into account the hygroscopic growth factors and by assuming a density for the dry aerosol particles, the volume size distributions determined by DMPS can be compared to the PM size distributions from the 11-stage MOUDI impactors. The correction for the difference between the mobility diameter

(DMA technique) and aerodynamic diameter (impactor technique) was made using the relation:

$$d_{ae} = d_{me} \cdot \sqrt{\rho_{wet}}$$

with d_{ae} = aerodynamic diameter, d_{me} = mobility diameter, and ρ_{wet} = wet density, assumed to be 1.2 kg dm^{-3}. Figures 3a–3c reports the PM size distributions obtained from DMPS integrated over the size intervals of the MOUDI and averaged over the time periods of the samplings with the impactors. The PM distributions were calculated from DMPS data assuming a dry density of 1.37 kg dm^{-3} [Rissler et al., 2006]. Comparison with the 11-stage MOUDI size distributions shows (1) a good agreement during the transition and wet periods, (2) broader distributions from MOUDI than for DMPS, especially in the dry period; (3) systematically higher concentrations from DMPS than from MOUDI in daytime conditions. The interpretation of the differences between MOUDI and DMPS PM size distributions is not straightforward, and the assumed dry density seems to have little effect on the discrepancies. The broader (and sometimes multimodal) distributions from MOUDI impactors can be partly attributed to external mixing of the hygroscopic and nonhygroscopic compounds in the particles, causing aerosol populations to have the same modal dry diameter but different ambient diameters. However, such explanation holds only for the samples collected at nighttime, when the RH was close to 100% and the aerosol could absorb a nontrivial amount of water, whereas during the day, when RH often fell below 50%, the particles showed a very limited hygroscopic growth [Rissler et al., 2006]. The higher concentrations provided by DMPS during daytime might reflect negative artifacts affecting sampling with the impactors, either because of the high ambient temperature (generally in the order of 35°C) promoting evaporation of semivolatile compounds, or because of the low relative humidity causing bouncing of dry particles on the impactor plates. The problems of lack of agreement between the DMA-based and the impactor-based aerosol measurements cannot fully be addressed here.

3.2. Size Distributions of the Main Inorganic Components of the Aerosol

[18] Figures 4a–4c show the size distributions of the main inorganic components of the aerosol resulting from the analysis of SDI and DLPI (for the N-containing compounds) samples. Because of the limited number of DLPI samples subjected to full chemical analysis, averages for the three periods of the campaign could not be calculated. Instead, samples representative for the three periods and for nocturnal and diurnal conditions were selected and their size distributions are reported in the figure, together with the PM size distributions from 11-stage MOUDI.

[19] With the exception of nitrate, sulphate, and potassium, the other inorganic components show size distributions with maxima either in the fine or in the coarse size range. We can distinguish between elements and ionic species enriched in the fine fraction and occurring with higher concentrations in the biomass-burning period ("pyrogenic" species), and other elements showing a main mode in the coarse size fraction and occurring in relatively constant concentrations
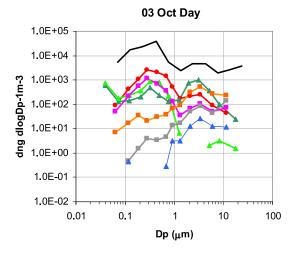
throughout the experiment. The latter include silicon, calcium, aluminium and iron (the last two not shown in the figure), plus other minor elements (titanium and manganese), which can all be associated with a single source of crustal particles, possibly suspended by the action of the wind and/or the convection generated by fires [Freitas et al., 2000]. Phosphorus, considered as a tracer of primary biogenic particles, shows similar size distributions as the crustal elements. The concentrations of phosphorus were lower than those of silicon and calcium in the dry period, while they were higher than those of calcium and comparable to those of silicon in the wet period. This finding indicates that at the onset of the wet season, primary biogenic particles increased their contribution to the coarse fraction relative to suspended soil particles. This is consistent with the combined effects of the decreasing number of fires and increasing humidity of soil, which hinder the resuspension of crustal particles. At the same time, plant productivity and emission of primary biogenic particles are expected to increase after the beginning of the rainy season.
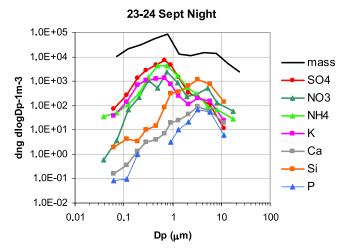
[20] Pyrogenic species include the aerosol chemical compounds produced during combustion, either directly emitted in the particulate phase or formed by subsequent oxidation and condensation of gaseous products. Sulphate, ammonium and, in the dry and transition periods potassium, are the most representative inorganic species of this category. Trace pyrogenic compounds (Zn, Se, Br, Rb, Pb) were also identified by PIXE analysis [Maenhaut et al., 2004]. Potassium, usually considered a marker for primary combustion products, shows size distributions with maxima in the supermicron size range during the wet period, suggesting that other sources of potassium, likely biogenic [Guyon et al., 2004a; Schkolnik et al., 2005], become important toward the wet season.

[21] The difference in the elemental composition of the fine and coarse aerosol in Rondônia and its interpretation on the basis of two main processes of aerosol emission, i.e., biomass burning and resuspension of soil particles, are in good agreement with the results provided by past experiments using filter-based techniques [Artaxo et al., 1998, 2002; Guyon et al., 2004b]. However, several previously unnoticed features in the size distributions of the inorganic components have been highlighted by the detailed analysis of the impactor data. A first important finding is that the maximum in the size distribution of pyrogenic compounds can be deconvoluted into two modes, with aerosol mean diameters of 0.3 and 0.7 μm, respectively, which correspond approximately to the two modes often observed in PM size distributions (see the section above). The two modes are more pronounced in the size distributions of potassium and sulphate, because of the larger number of stages of the SDI and DLPI compared to the 11-stage MOUDI. The occurrence of two modes in the submicrometer size range has frequently been attributed to the production of large accumulation-mode particles in nonprecipitating clouds [Ricard et al., 2002]. During this experiment, the activation of aerosol particles within nonprecipitating cumuli in the afternoon and within the nocturnal fogs may be responsible for the appearance of a "droplet mode" at a diameter of 0.7 μm.
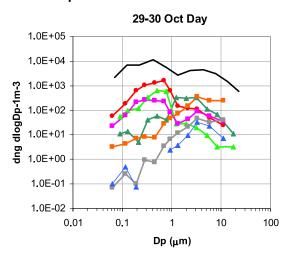
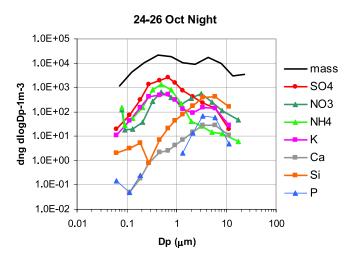[22] Size distributions in the supermicron size range always exhibit a single broad maximum. However, the
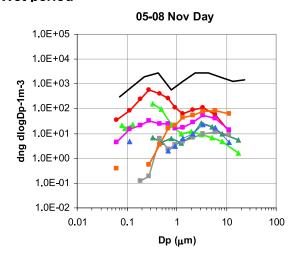
Dry period

Transition period

Wet period

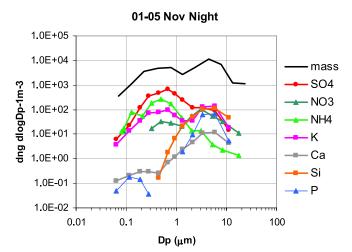**Figure 4**

composition of coarse particles is likely to be a mixture of inorganic compounds originating from different sources. In particular, there is evidence of the adsorption of inorganic vapours produced by biomass burning onto primary particles made up of crustal material and phosphorus-rich biogenic organic material. Indeed, unlike ammonium, whose size distribution remains always confined to the submicron fraction, sulphate and nitrate size distributions also show a distinct coarse mode. In the case of the most volatile species (nitrate), during the transition and wet periods, the coarse mode is generally even higher than the fine mode. These data suggest that the primary coarse particles contain alkaline material, which promotes the condensation of sulphur dioxide and nitric acid. Therefore the condensation of semivolatiles onto the coarse particles competed with that on the submicrometer particles, the former becoming dominant for nitrate after the end of the dry season, when the concentrations of fine aerosols dropped considerably.

3.3. Size Distributions of the Main Aerosol Carbon Classes

[23] Size segregated TC data were obtained from the analysis of selected 11-stage MOUDI samples for the dry period and of DLPI for the transition and wet periods. Size distributions of EC have not been determined. Examples of TC size distributions, together with the PM distributions for the same samples, are shown in Figures 5a–5c. Generally, there is a close correlation between the size spectra of PM and TC in the submicrometer size range. The TC/PM ratio for the fine fraction of the aerosol is 0.41 ± 0.11, on average, when calculated on the analysed MOUDI samples. These findings strongly support previous observations that the fine particulate matter produced by biomass burning is largely carbonaceous. Little or no difference was observed in the TC/PM ratio between the size ranges corresponding to the condensation mode and the droplet mode [*Maenhaut et al.*, 2004], indicating that TC was the primary constituent of the fine particles throughout the submicron size range. The size distribution of TC is different from that of PM in the supermicron size range, where a substantial fraction of the mass is expected to be accounted for by inorganic crustal material. This is particularly evident in the samples from the dry period. The TC distributions determined by EGA analysis on the DLPI samples from the transition and wet periods essentially follow the same behaviour observed for the MOUDI samples, suggesting that fine particles continue to be substantially carbonaceous in nature also after the end of the biomass-burning period.

[24] Size distributions of the water-soluble (i.e., water-extractable) organic compounds (WSOC) were determined for BI samples. Average distributions for the various periods are reported in Figure 6. The WSOC size distributions qualitatively follow those of TC, with a distinct mode in the fin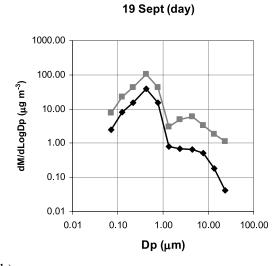e fraction in all periods. Because of the low size resolution of the BI, the occurrence of a WSOC coarse mode cannot be readily noticed in most samples. However, it can be noted that the concentration of WSOC in the particles of the supermicron size range is relatively higher during the night in the transition and wet periods. In the dry period, the standard deviation of the concentrations is higher compared to the other two periods, following the analogue variations observed for fine PM. Compared to the size distributions of PM and TC, the mode of WSOC in the submicron size range is shifted toward larger sizes, being within the $0.42–1.2$ μm interval in all periods, with the exception of the wet period daytime samples. The analysis of specific classes of WSOC by IC on 8-stage MOUDI samples [*Falkovich et al.*, 2005] also supports an enrichment of the polar fraction of OC in the size range between 0.4 and 1 μm, i.e., at larger diameters compared to the modal size of PM and TC.

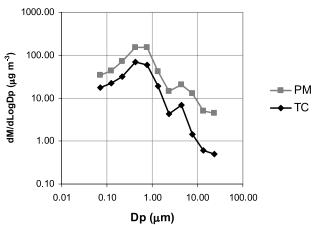### 3.4. Size Distributions of Key Aerosol Organic Tracers

[25] Organic chemical analyses were able to speciate at the molecular level about $6–8\%$ of the measured TC [*Decesari et al.*, 2006]. The identified organic compounds encompass polyhydroxylated compounds, with levoglucosan as the most abundant species, short-chain aliphatic carboxylic acids with oxalic acid as the most abundant compound, and, finally, benzoic and phenolic acids. Functional group analysis by proton nuclear magnetic resonance (H NMR) spectroscopy [*Tagliavini et al.*, 2006] indicates that saturated aliphatic compounds and many aromatics were not detected by individual compound analysis, while significant amounts of the compounds carrying C-OH and COOH groups were identified at the molecular level [*Decesari et al.*, 2006]. Furthermore, only low molecular weight species could be efficiently determined by GC/MS and IC methods, while the medium-to-high molecular weight fraction, mostly accounted for by humic-like substances, could be characterized only by functional group analysis [*Tagliavini et al.*, 2006]. Among the identified WSOC, many were considered as molecular markers for specific sources of organic material. For example, levoglucosan and the other sugar anhydrides are known tracers of biomass combustion [*Simoneit et al.*, 1999], sugars and sugar alcohols enter the aerosol phase by direct emission from the biota [*Graham et al.*, 2003] or because of the resuspension of organic-rich soil particles [*Simoneit et al.*, 2004], and malic acid is believed to be an intermediate photo-oxidation product of unsaturated fatty acids [*Kawamura et al.*, 1996]. Finally, methyltetrols and C_5 alkene triols were recently identified as products of isoprene photo-oxidation [*Claeys et al.*, 2004a, 2004b; *Wang et al.*, 2005]. A full discussion of the results of the size segregated organic analyses on 8-stage and 11-stage MOUDI samples collected during the SMOCC campaign is given by *Falkovich et al.* [2005], *Schkolnik et al.* [2005] and M. Claeys et al. (in preparation, 2006).

Figure 4. Size distributions of inorganic ions and elements for selected samples collected during nighttime and daytime in the dry (a), transition (b) and wet periods (c). Nitrate and ammonium size distributions were derived from DLPI impactors. All the other chemical species were determined for SDI samples. Sulphate concentrations were calculated as three times the concentrations of elemental sulphur determined by PIXE on the SDI substrates. PM size distributions from MOUDI for the same samples are also reported.
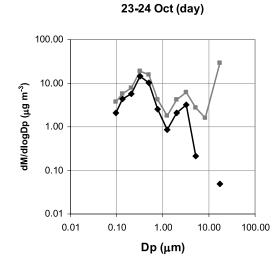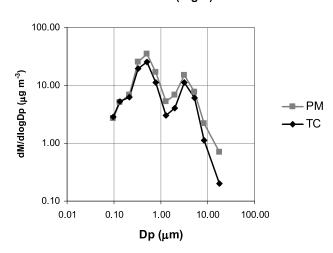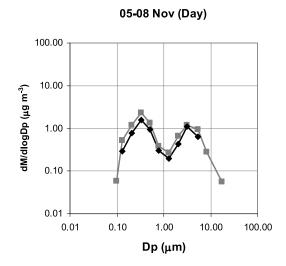
a)

19 Sept (day)

19 - 20 Sept (night)

b)

23-24 Oct (day)

24-26 Oct (Night)

c)

05-08 Nov (Day)

01-05 Nov (Night)

Figure 5

Dry period

Transition period

Wet period

Figure 6. Average WSOC size distributions from the 5-stage BI for the dry, transition and wet periods.

[26] Despite the fact that the organic compounds identified at the molecular level add up to a relatively small percentage of total OC, their total mass is of the same order of magnitude as that of inorganic ions [*Falkovich et al.*, 2005; *Trebs et al.*, 2005]. Therefore in principle, organic tracer analysis on the SMOCC samples is as important for the source apportionment of PM as the analysis of the inorganic composition. Figures 7a and 7b show the size distributions of some organic tracers representative of the main sources of OC identified in the various periods. The data refer to GC/MS analyses performed on 11-stage MOUDI samples and PM is shown in the figure for the same samples. Mannitol exhibits a size distribution with a single mode in the supermicron size range in all periods. In fact, sugar alcohols are produced by fungal spores which can be directly emitted in the atmosphere or associated with plant debris and soil particles [*Graham et al.*, 2003; *Simoneit et al.*, 2004]. Conversely, biogenic organic compounds formed by secondary processes, like methyltetrols and malic acid, are enriched in submicrometer particles. The same is true for the biomass-burning products like levoglucosan. By contrast, both levoglucosan and malic acid exhibit a bimodal distribution during the wet period, with a coarse mode which is slightly shifted toward larger sizes compared to that of mannitol.

[27] These findings suggest that the previous conclusions concerning the nature of OC in the fine and in the coarse modes must be treated with caution for two reasons: (1) not all submicrometer particles are produced by biomass burning, and biogenic compounds are common constituents in all three periods [see also *Graham et al.*, 2002, 2003]; (2) coarse particles actually include biogenic material derived from plant debris, plant pollen and fungal spores but, in the wet period, when the concentrations of the fine particles is small, semivolatile compounds originating from both biomass burning and biogenic sources are present as condensed material onto the coarse particles. Therefore the simple interpretation of the modality of PM, with the fine particles derived from biomass burning and the coarse ones from natural background, cannot be fully sustained on the basis of the present results.

3.5. Size-Segregated Chemical Mass Balance of the Aerosol

[28] In the previous section, the size distributions of the chemical constituents of the aerosol were compared to that of PM with respect to modal size and shape. For a more quantitative comparison between the concentrations of PM and those of the analysed chemical compounds, a size-segregated mass balance of the aerosol must be calculated, provided that all concentrations are available for the same size intervals. The results of the mass balance calculation performed on the 8-stage MOUDI samples, for which both PM and the concentrations of inorganic ions and organic tracers determined by IC are available, are discussed by *Falkovich et al.* [2005]. Here, we provide a mass balance

Figure 5. Size distributions of total carbon (TC) for selected samples collected during nighttime and daytime in the dry (a), transition (b) and wet periods (c). Dry period samples were collected by 11-stage MOUDI and analysed with a Shimadzu TOC analyser with Solid Sample Module (SSM). Samples for the transition and wet periods were collected by DLPI and analysed by EGA. PM size distributions for the same samples are also reported.
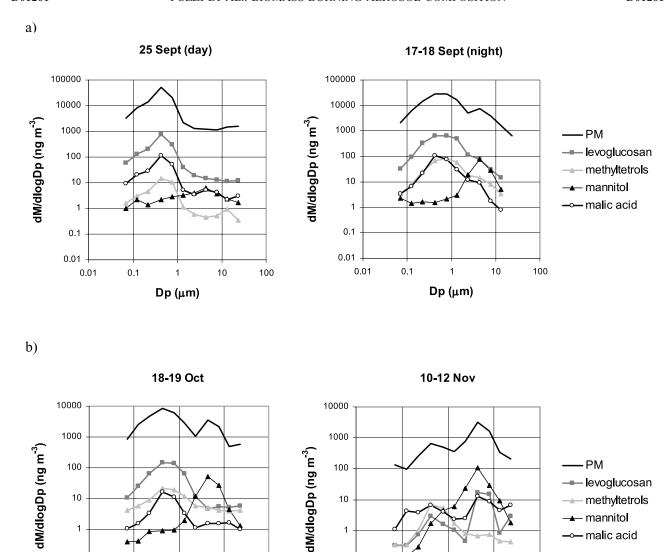
a)

b)

Figure 7. Size distributions of the main identified organic compounds determined by GC/MS analysis for 11-stage MOUDI samples. (a) Dry period (day and night conditions), (b) transition and wet periods. PM size distributions for the same samples are also reported.

involving both inorganic (soluble and insoluble) compounds and the main carbon classes. Unfortunately, there were no impactor samples on which a complete determination of PM, TC classes, inorganic ions and elements could be performed, and the data had therefore to be retrieved from the analysis of samples from different impactor types. To this aim, the concentrations determined on the higher-resolution multistage impactors (SDI, MOUDI and DLPI) were integrated into the BI cut-offs: 0.05–0.14, 0.14–0.42, 0.42–1.2, 1.2–3.5, 3.5–10 μm. The BI data were divided by the size-resolved ratios $PM_{(BI)}/PM_{(MOUDI)}$ for the dry period samples in order to account for the different sampling efficiencies of the impactors. For the transition and wet periods, the $[SO_{4(BI)}]/[SO_{4(DLPI)}]$ ratios were used to

correct the BI data, since aluminium foils for PM determination were not mounted on the BI during the last part of the campaign. The SDI data concentrations of crustal elements were also corrected using the factor $[K_{(BI\ corrected)}]/[K_{(SDI)}]$. Crustal elements were then converted into mineral fractions on the basis of the equation: [crustal material] = 1.16 (1.90Al + 2.15Si + 1.41Ca + 1.67Ti + 2.09Fe) [*Maenhaut et al.*, 2002]. Finally, the mass of water-soluble organic compounds (i.e., the water-soluble organic mass, WSOM) characterized by chromatographic techniques and NMR functional group analysis was calculated from the measured carbon concentrations and organic matter (OM) to OC ratios on the basis of the average chemical composition [*Decesari et al.*, 2006]. For the uncharacterized WSOC (ranging from

5 to 50% of the total), a conversion factor of 1.7 was used. The resulting size-resolved aerosol chemical mass budget for the three periods of the campaign and for day and night conditions is reported in Tables 2a–2c. The TC concentrations during the transition and wet periods are likely affected by instrumental biases; systematically higher TC/PM ratios were obtained for the DLPI samples analysed by the EGA technique compared to the 11-stage MOUDI samples analysed by the solid TOC analyser. For this reason, the estimation of the non-water-soluble carbon mass was not attempted in this study. Figure 8 reports the mass balance of the aerosol expressed as a percentage of PM accounted for by WSOM, inorganic ions (details in Figure 9) and the mineral fraction in the five size intervals of the BI. The unaccounted mass, representing some 0 to 60%, includes insoluble TC species (insoluble OC + EC), and, possibly, aerosol water. However, bon the basis of the hygroscopicity data [*Rissler et al.*, 2006], the amount of water in the samples conditioned for gravimetry (RH = 30 to 50%; see Table 1) represents less than 10% of the particle volume. The mean ratio EC/TC in the fine fraction during the dry and transition periods was 0.12 ± 0.04, with no significant differences between these two periods. With a TC/PM ratio of 0.41, this corresponds to an EC mass fraction of $5.0 \pm 1.6\%$.

[29] The mineral fraction is a major aerosol component in the supermicron size range, accounting for 5 to 40% of PM. Inorganic ions represent from 5 to 20% of PM, and show an enrichment in the intermediate size intervals, always peaking in the $0.42-1.2$ μm size range, and they have a significantly lower contribution to PM in the supermicron size range during the wet period. Interestingly, the maximum percentage of PM accounted for by inorganic ions appears in the size interval which includes the "droplet" mode evident in the size distributions of PM, potassium and sulphate. Clearly, WSOC are the main contributors to the aerosol mass balance in the submicron size range during all periods of the experiment, with maxima in the lowest size range ($0.05-0.14$ μm) and in the $0.42-1.2$ μm interval. It should be noted that the uncertainty associated with the analysis of the very lightly loaded samples of the wet period may be partly responsible for the very high contribution of WSOM to PM with respect to the lowest size range.

[30] Despite some differences observed between the various periods of the experiment and diurnal/nocturnal conditions, we can summarize the mass balance of the aerosol analyzed within LBA-SMOCC as follows:

[31] 1. Particles belonging to the lowest size range ($<\sim0.4$ μm) are characterized by a large fraction of PM consisting of water-soluble and insoluble carbonaceous species, while inorganic ions (mainly potassium and ammonium sulphates) represent only $5-15\%$ of that size range.

[32] 2. Particles in the size range $0.42-1.2$ μm exhibit a completely different composition, characterized by the highest contribution from water-soluble compounds (both inorganic and organic). WSOC are still dominant, but inorganic ions (with ammonium sulphate and, sometimes, ammonium nitrate, as major species) may account for up to 20% of the mass.

[33] 3. Coarse aerosols are characterized by variable amounts of WSOC, inorganic ions (with sodium nitrate as the most abundant compound) and crustal material, plus a fraction of undetermined insoluble organic species, which dominate the composition during the transition and wet periods.

[34] Clearly, despite the relatively simple PM size distributions showing one or two distinct modes in the fine and coarse fractions, the chemical composition varied quite significantly as a function of aerosol particle size. Therefore a single homogeneous aerosol composition, or even a composition differentiated between fine and coarse fractions cannot be justified for model applications.

4. Evolution of the Size-Segregated Aerosol Chemical Composition From the Dry (Biomass Burning) Period to the Onset of the Wet Season

[35] In the previous sections, average size-segregated compositions of the aerosol collected at the FNS site were obtained for the three main periods of the campaign, separately for samples collected at daytime and nighttime. However, the trend of PM_{10} (Figure 2a) clearly shows significant variability within each period, especially in the dry period, when the accumulation of smoke particles was occasionally interrupted by sparse but intense precipitation events. After dry conditions were established again, PM_{10} levels increased within a couple of days of the propagation of fires. Such changes in rainfall rate and burning activity are, therefore likely to affect the chemical composition of the aerosols.

[36] In this second part of the study, an attempt is made to follow the evolution of the aerosol chemical composition following changes in rainfall rate and source strength, by isolating three subperiods representative of the conditions occurring in the dry, transition and wet periods. A summary of the main meteorological parameters for the selected subperiods is provided in Table 3. Subperiods 1 and 2 had similar values of temperature extremes (both minimum and maximum), while the period from 30 October to 15 November was characterized by much lower maximum temperatures. RH followed the rainfall distribution, increasing from the first (driest) subperiod to the third one (wetter). Solar radiation was highest in the second subperiod (21– 29 October) and lowest in the third one.

4.1. Subperiod 1 (14–22 September 2002)

[37] During this period, the region was very dry (no rainfall at all), smoke was constantly produced by widespread local and regional fires and maximum temperatures at the surface reached 34–35°C. The height of the CBL reached 1800–2000 m in the middle of the afternoon, associated with maximum solar radiation fluxes of 800– 850 W m^{-2}. RH values ranged from 100% (with foggy conditions) at nighttime till sunrise, to around 40–50% in the early afternoon.

4.1.1. High Time Resolution Aerosol Measurements

[38] Just before the period considered here, the passage of a cold front caused a considerable reduction of PM_{10} concentrations at the FNS station, down to 20–30 μg m^{-3}, i.e., well below the average for the dry period. Starting on September 16, smoky conditions were observed at the FNS site, causing a marked reduction in visibility during the following days. The $PM_{2.5}$ time trends from TEOM indicate that concentrations increased steadily from 16 to

Table 2a. Concentrations of Size-Resolved Aerosol Chemical Components for the Three Periods of the Campaign: Dry period[a]

AD, μm	Minor Ions, μg m⁻³ Mean	Standard Deviation	NO₃⁻, μg m⁻³ Mean	Standard Deviation	SO₄⁼, μg m⁻³ Mean	Standard Deviation	NH₄⁺, μg m⁻³ Mean	Standard Deviation	K⁺, μg m⁻³ Mean	Standard Deviation	WSOC, μgC m⁻³ Mean	Standard Deviation	WSOM, μg m⁻³ Mean	Standard Deviation	TC MOUDI, μgC m⁻³ Mean	Standard Deviation	Mineral Fraction SDI, μg m⁻³ Mean	Standard Deviation	PM, μg m⁻³ Mean	Standard Deviation
									Night											
0.05–0.14	0.02 *0.00*	0.03	0.16 *0.01*	0.17	0.22 *0.02*	0.16	0.14 *0.01*	0.13	0.17 *0.02*	0.12	3.41 *0.34*	2.31	5.73 *0.58*	3.89	8.03 *0.45*	0.99	0.009 *0.00*	0.008	10.32	5.38
0.14–0.42	0.03 *0.00*	0.03	0.45 *0.01*	0.45	0.55 *0.03*	0.27	0.34 *0.01*	0.22	0.40 *0.02*	0.26	6.63 *0.25*	4.10	11.92 *0.45*	7.39	22.44 *0.47*	2.81	0.015 *0.00*	0.009	27.49	15.22
0.42–1.2	0.11 *0.00*	0.10	1.63 *0.04*	1.19	1.99 *0.06*	0.78	1.58 *0.04*	0.85	0.82 *0.02*	0.46	13.68 *0.36*	8.05	25.28 *0.67*	15.02	26.96 *0.46*	7.55	0.220 *0.01*	0.167	37.62	21.46
1.2–3.5	0.12 *0.02*	0.08	0.25 *0.03*	0.22	0.18 *0.02*	0.18	0.14 *0.02*	0.17	0.08 *0.01*	0.07	1.66 *0.22*	1.43	2.83 *0.38*	2.44	3.01 *0.31*	1.54	1.340 *0.18*	1.000	7.44	5.07
3.5–10	0.19 *0.02*	0.14	0.26 *0.02*	0.20	0.06 *0.01*	0.05	0.04 *0.00*	0.04	0.09 *0.01*	0.04	1.75 *0.18*	0.72	2.95 *0.30*	1.21	1.81 *0.16*	0.26	2.002 *0.21*	1.364	9.77	2.33
									Day											
0.05–0.14	0.01 *0.00*	0.01	0.09 *0.01*	0.13	0.33 *0.05*	0.28	0.15 *0.02*	0.06	0.13 *0.02*	0.05	2.57 *0.36*	1.26	4.58 *0.65*	2.26	3.18 *0.28*	2.03	0.012 *0.00*	0.010	7.12	3.78
0.14–0.42	0.02 *0.00*	0.01	0.18 *0.01*	0.27	0.78 *0.04*	0.40	0.38 *0.02*	0.19	0.33 *0.02*	0.16	6.74 *0.34*	3.79	12.31 *0.63*	7.02	11.74 *0.40*	5.39	0.020 *0.00*	0.013	19.91	12.08
0.42–1.2	0.07 *0.01*	0.12	0.31 *0.02*	0.33	0.94 *0.08*	0.47	0.55 *0.04*	0.32	0.32 *0.02*	0.18	5.95 *0.43*	3.66	10.93 *0.78*	6.86	10.71 *0.52*	5.29	0.138 *0.01*	0.093	13.99	9.30
1.2–3.5	0.15 *0.04*	0.08	0.15 *0.04*	0.12	0.12 *0.03*	0.11	0.05 *0.01*	0.08	0.05 *0.01*	0.09	1.00 *0.19*	1.44	1.74 *0.33*	2.60	6.03 *0.20*	10.95	0.813 *0.24*	0.479	4.78	5.84
3.5–10	0.20 *0.04*	0.10	0.30 *0.05*	0.36	0.17 *0.02*	0.46	0.10 *0.01*	0.37	0.08 *0.01*	0.19	1.38 *0.16*	3.08	2.45 *0.27*	5.71	6.95 *0.15*	13.34	1.180 *0.25*	0.614	6.68	7.87

[a]Dry period and for day and night conditions. Data refer to the analysis of the BI sample set, unless otherwise indicated. The concentrations determined on the high-resolution multistage impactors (SDI, MOUDI, DLPI) have been summed into the size ranges defined by the BI cut-offs. Mean concentrations are reported together with standard deviations and the PM fractions (in *italics*) accounted for by each chemical species. For the transition and wet period samples, PM fractions are calculated with respect to $PM_{(DLPI)}$ concentrations. Minor ions = $Cl^- + Na^+ + Mg^{2+} + Ca^{2+}$.

Table 2b. Concentrations of Size-Resolved Aerosol Chemical Components for the Three Periods of the Campaign: Transition Period[a]

AD, μm	Minor Ions, μg m⁻³		NO₃⁻, μg m⁻³		SO₄=, μg m⁻³		NH₄⁺, μg m⁻³		K⁺, μg m⁻³		WSOC, μgC m⁻³		WSOM, μg m⁻³		TC DLPI, μgC m⁻³		Mineral Fraction SDI, μg m⁻³		PM DLPI, μg m⁻³		PM MOUDI, μg m⁻³	
	Mean	Standard Deviation	Mean	Standard Deviation	Mean	Standard Deviation	Mean	Standard Deviation	Mean	Standard Deviation	Mean	Standard Deviation	Mean	Standard Deviation	Mean	Standard Deviation	Mean	Standard Deviation	Mean	Standard Deviation	Mean	Standard Deviation
Night																						
0.05–0.14	0.002 *0.00*	0.001	0.006 *0.00*	0.004	0.049 *0.03*	0.025	0.015 *0.01*	0.007	0.030 *0.02*	0.014	0.60 *0.30*	0.31	1.17 *0.59*	0.61	1.20 *1.07*		0.001 *0.00*	0.000	1.12		1.91	1.20
0.14–0.42	0.008 *0.00*	0.003	0.044 *0.01*	0.014	0.498 *0.08*	0.146	0.175 *0.03*	0.039	0.171 *0.02*	0.051	2.97 *0.34*	0.97	5.72 *0.65*	1.91	5.74 *0.81*		0.008 *0.00*	0.001	7.06		7.87	3.11
0.42–1.2	0.026 *0.00*	0.018	0.151 *0.02*	0.073	0.905 *0.10*	0.399	0.364 *0.04*	0.142	0.213 *0.02*	0.079	3.59 *0.35*	1.56	6.74 *0.65*	2.94	6.87 *0.70*		0.085 *0.01*	0.025	9.85		8.76	3.56
1.2–3.5	0.115 *0.03*	0.064	0.146 *0.04*	0.044	0.146 *0.04*	0.051	0.038 *0.01*	0.014	0.044 *0.01*	0.004	0.84 *0.21*	0.06	1.67 *0.41*	0.10	2.89 *0.68*		0.332 *0.11*	0.118	4.25		3.92	0.88
3.5–10	0.073 *0.03*	0.035	0.124 *0.05*	0.033	0.017 *0.00*	0.015	0.004 *0.00*	0.001	0.044 *0.01*	0.009	0.85 *0.32*	0.31	1.59 *0.58*	0.57	2.29 *0.74*		0.594 *0.29*	0.316	3.09		5.18	1.06
Day																						
0.05–0.14	0.002 *0.00*	0.002	0.001 *0.00*	0.001	0.055 *0.01*	0.058	0.026 *0.01*	0.013	0.024 *0.01*	0.012	0.42 *0.24*	0.15	0.79 *0.46*	0.30	1.13 *0.72*	0.17	0.002 *0.00*	0.000	1.56	0.02	1.57	0.76
0.14–0.42	0.012 *0.00*	0.005	0.008 *0.00*	0.002	0.391 *0.06*	0.138	0.134 *0.02*	0.038	0.103 *0.02*	0.039	1.72 *0.29*	0.37	3.24 *0.55*	0.72	4.36 *0.84*	0.13	0.016 *0.00*	0.006	5.26	0.61	3.47	1.06
0.42–1.2	0.015 *0.00*	0.004	0.012 *0.00*	0.004	0.564 *0.10*	0.235	0.201 *0.04*	0.074	0.101 *0.02*	0.031	1.59 *0.33*	0.35	2.93 *0.60*	0.66	2.84 *0.67*	0.65	0.126 *0.03*	0.034	4.23	0.73	3.91	1.08
1.2–3.5	0.152 *0.05*	0.078	0.136 *0.05*	0.067	0.102 *0.01*	0.089	0.004 *0.00*	0.000	0.023 *0.01*	0.003	0.38 *0.17*	0.08	0.72 *0.32*	0.15	0.90 *0.45*	0.12	0.334 *0.19*	0.061	2.01	0.06	1.72	0.25
3.5–10	0.069 *0.03*	0.047	0.099 *0.05*	0.066	0.060 *0.01*	0.088	0.002 *0.00*	0.001	0.016 *0.01*	0.000	0.20 *0.14*	0.03	0.35 *0.24*	0.07	0.37 *0.30*	0.16	0.616 *0.49*	0.160	1.27	0.04	1.66	0.24

[a]As in Table 2a, but for the transition period.

Table 2c. Concentrations of Size-Resolved Aerosol Chemical Components for the Three Periods of the Campaign: Wet Period[a]

AD, μm	Minor Ions, μg m^{-3}		NO$_3^-$, μg m^{-3}		SO$_4^=$, μg m^{-3}		NH$_4^+$, μg m^{-3}		K$^+$, μg m^{-3}		WSOC, μgC m^{-3}		WSOM, μg m^{-3}		TC DLPI, μgC m^{-3}		Mineral fraction SDI, μg m^{-3}		PM DLPI, μg m^{-3}		PM MOUDI, μg m^{-3}	
	Mean	Standard Deviation	Mean	Standard Deviation	Mean	Standard Deviation	Mean	Standard Deviation	Mean	Standard Deviation	Mean	Standard Deviation	Mean	Standard Deviation	Mean	Standard Deviation	Mean	Standard Deviation	Mean	Standard Deviation	Mean	Standard Deviation
											Night											
0.05–0.14	0.008 *0.01*	0.008	0.004 *0.01*	0.004	0.012 *0.04*	0.012	0.010 *0.02*	0.010	0.008 *0.02*	0.008	0.22 *0.57*	0.22	0.41 *1.08*	0.41	0.40 *1.38*	0.40	0.003 *0.00*	0.003	0.38	0.38	0.38	0.38
0.14–0.42	0.004 *0.00*	0.004	0.029 *0.02*	0.029	0.106 *0.06*	0.106	0.056 *0.04*	0.056	0.024 *0.02*	0.024	0.67 *0.44*	0.67	1.27 *0.73*	1.27	1.46 *0.84*	1.46	0.003 *0.00*	0.003	1.56	1.56	1.65	1.65
0.42–1.2	0.003 *0.00*	0.003	0.091 *0.05*	0.091	0.163 *0.09*	0.163	0.104 *0.06*	0.104	0.036 *0.02*	0.036	0.91 *0.49*	0.91	1.69 *0.70*	1.69	1.25 *0.66*	1.25	0.011 *0.01*	0.011	1.90	1.90	1.88	1.88
1.2–3.5	0.016 *0.01*	0.016	0.021 *0.01*	0.021	0.037 *0.02*	0.037	0.019 *0.01*	0.019	0.019 *0.01*	0.019	0.33 *0.17*	0.33	0.59 *0.23*	0.59	1.61 *0.78*	1.61	0.112 *0.07*	0.112	2.01	2.01	2.12	2.12
3.5–10	0.016 *0.01*	0.016	0.011 *0.01*	0.011	0.015 *0.01*	0.015	0.002 *0.00*	0.002	0.030 *0.01*	0.030	0.44 *0.18*	0.44	0.81 *0.24*	0.81	1.77 *0.85*	1.77	0.204 *0.13*	0.204	2.28	2.28	4.77	4.77
											Day											
0.05–0.14	0.001 *0.00*	0.001	0.001 *0.00*	0.001	0.013 *0.05*	0.013	0.004 *0.02*	0.004	0.003 *0.01*	0.003	0.07 *0.27*	0.07	0.14 *0.54*	0.14	0.04 *0.38*	0.04	0.006 *0.02*	0.006	0.21	0.21	0.21	0.21
0.14–0.42	0.007 *0.00*	0.007	0.005 *0.00*	0.005	0.115 *0.13*	0.115	0.043 *0.05*	0.043	0.011 *0.01*	0.011	0.35 *0.35*	0.35	0.64 *0.66*	0.64	0.47 *0.67*	0.47	0.003 *0.00*	0.003	1.31	1.31	1.05	1.05
0.42–1.2	0.002 *0.00*	0.002	0.002 *0.00*	0.002	0.085 *0.18*	0.085	0.027 *0.06*	0.027	0.010 *0.02*	0.010	0.19 *0.35*	0.19	0.37 *0.68*	0.37	0.24 *0.72*	0.24	0.029 *0.07*	0.029	1.03	1.03	0.97	0.97
1.2–3.5	0.012 *0.02*	0.012	0.007 *0.01*	0.007	0.018 *0.04*	0.018	0.003 *0.01*	0.003	0.008 *0.01*	0.008	0.10 *0.18*	0.10	0.19 *0.36*	0.19	0.28 *0.80*	0.28	0.095 *0.22*	0.095	0.59	0.59	0.84	0.84
3.5–10	0.007 *0.01*	0.007	0.010 *0.02*	0.010	0.006 *0.01*	0.006	0.001 *0.00*	0.001	0.006 *0.01*	0.006	0.07 *0.15*	0.07	0.12 *0.29*	0.12	0.22 *0.65*	0.22	0.128 *0.32*	0.128	0.45	0.45	0.97	0.97

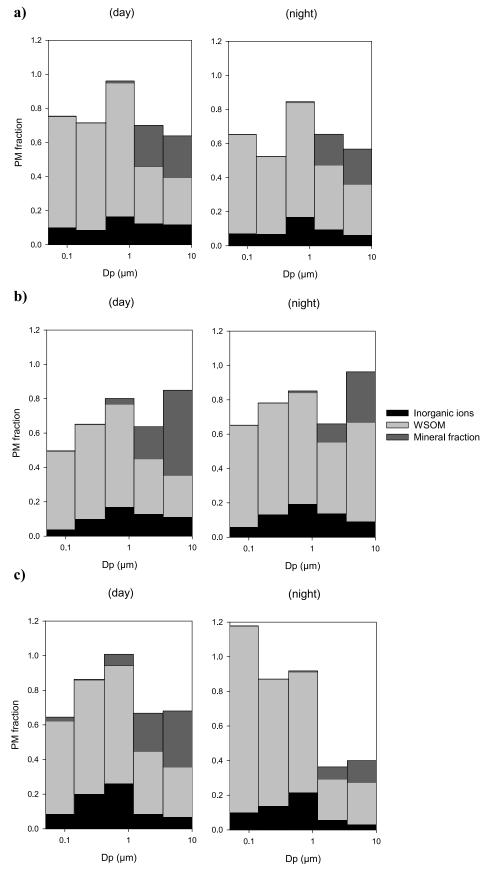[a]As in Table 2a, but for the wet period.

Figure 8

21 September (Figure 10). The concentrations of PM_{10} deviated very little from that of $PM_{2.5}$ ($r^2 = 0.97$). In this period, the fairly constant ratio between the concentrations of CO and $PM_{2.5}$ (0.080 ± 0.014, $\mu g\ m^{-3}\ ppb^{-1}$) indicates that (1) fires were essentially responsible for the observed aerosol levels; (2) aerosols did not experience any important loss, while their concentration was simply dependent on the intensity of the sources, the transport to/from the area and the dynamics of the boundary layer. During the biomass-burning period, the concentrations of pyrogenic trace gases and of PM showed clear diurnal oscillations, which are linked to the cycle of the boundary layer. This means that combustion sources were active throughout the day and the night, and that the concentration peaks observed at nighttime are due to the accumulation of freshly produced aerosol particles in the nocturnal surface layer. Concentrations dropped after sunrise because of the increase in the height of the mixing layer. During the day, the emissions from new fires led to a very slight increase in the concentrations since the boundary layer was thicker and well mixed. At the same time, more aged particles from the upper layers, which had been isolated from the surface during the night, entered the boundary layer and reached the ground. Therefore the aerosol at the ground level was a mixture of fresh and aged particles during the day, whereas the increase in the nocturnal aerosol concentrations was only due to fresh aerosol emitted after sunset.

[39] The concentrations of aerosol TC from the carbon monitor follow exactly the same trend as $PM_{2.5}$, confirming that biomass-burning particles are mainly carbonaceous (Figure 10). The carbon monitor discriminates between refractory carbon evolving above 350°C and the more volatile carbon species. The ratio between the refractory carbon and TC was ~0.3, with no clear trend between 14 and 16 September. On subsequent days, after the increase of biomass-burning activities, this ratio oscillates between 0.2 at night and 0.3 during the day. The enrichment in refractory carbon during the day can be due to widespread flaming combustion, peaking in the afternoon, whereas more frequent smoldering conditions typically occurred during the night. Smoldering combustion is known to emit particles with a lower refractory carbon to TC ratio compared to flaming conditions [Rau, 1989]. Photochemical reactions can also contribute to the formation of refractory carbon during the day [Hoffer et al., 2005]. In any case, the measurements provided by the carbon monitor clearly indicate that the carbonaceous material in freshly produced particles overnight has a different composition compared to the more aged one of daytime aerosol.

4.1.2. Time-Integrated Measurements

[40] For the 14–22 September period, impactor measurements integrated over 12 h are available from the 11-stage MOUDI, SDI and the BI. Sampling with several filter devices was also performed in parallel with the impactors. The trend of $PM_{1.8}$ from MOUDI is consistent with the TEOM $PM_{2.5}$ concentration trend, showing large diurnal variations after 15 September. Average nocturnal concen-

trations increased four times from 14 to 20 September, while the increase in the average daytime concentrations is of ~2.5 times. 21 September was atypical, showing much higher daytime concentrations compared to the previous days. The high time resolution measurements by TEOM and the carbon monitor (Figure 10) suggest that the evolution of the mixing layer and the consequent dispersal of the nocturnal aerosol were retarded that day until afternoon. Therefore the time-integrated impactor and filter samples for 21 September likely contained aerosol particles of the nocturnal surface layer of the night before.

[41] The TC and WSOC in $PM_{2.5}$ determined on HVDS samples follow the same trend as fine PM (Figure 11a) ($r^2 = 0.93$ for both $TC_{(HVDS)}$ vs. $PM_{1.8(MOUDI)}$ and $WSOC_{(HVDS)}$ vs. $PM_{1.8(MOUDI)}$), confirming the evidence from the mass balance results (Figure 8) that the fine PM during the biomass-burning period was constituted mostly by organic compounds. Also the concentrations of the major inorganic species, determined in fine aerosol samples from filter and impactor measurements, increased after 15 September (Figure 11b), indicating that they are also products of biomass burning. However, while the trend of potassium concentration overlaps with those of PM, TC and WSOC ($r^2 = 0.92$ for $K_{(SDI)}$ vs. $PM_{1.8(MOUDI)}$), sulphate and nitrate profiles show a weaker correlation ($r^2 = 0.64$ and 0.86, respectively, for $sulphate_{(SDI)}$ vs. $PM_{1.8(MOUDI)}$ and $nitrate_{(BI)}$ vs. $PM_{1.8(MOUDI)}$). In the case of nitrate in $PM_{1.2}$ (from the sum of the concentrations in the first three stages of the BI), only the nighttime concentrations underwent a sudden increase, starting on the night of 16–17 September and peaking at $4\ \mu g\ m^{-3}$. Conversely, the daytime concentrations remained below $0.5\ \mu g\ m^{-3}$ throughout the whole period, with the exception of 21 September. The stable meteorological conditions encountered at the FNS from 15 to 21 September were characterized by marked differences of T and RH values between day and night. This caused aerosol nitrate to evaporate forming gaseous nitric acid during daytime, followed by recondensation of nitric acid and ammonia onto particles during the night [Trebs et al., 2004, 2005]. Sulphate in $PM_{1.7}$ (from SDI) shows an average increase of only a factor of two (from 2 to $4\ \mu g\ m^{-3}$). The trend of sulphate concentrations shows no diurnal variation and reflects that of its precursor in the gas phase, sulphur dioxide [Trebs et al., 2004].

[42] From the analysis of trends in the concentrations of PM and the main carbonaceous and inorganic components, it can be concluded that biomass-burning activities were responsible for the increase in both inorganic and organic compounds concentrations in the aerosol observed from 16 to 21 September. However, the increase of PM was driven mostly by TC, whereas only a limited increase in sulphate concentrations was observed, and nitrate contributed only at nighttime. Regression analysis of sulphate concentrations versus fine PM levels indicates that in conditions of very low PM concentrations, there is a sulphate "background" of ~$2\ \mu g\ m^{-3}$. A good correlation between TC, PM, potassium and CO was found for both

Figure 8. Size-segregated aerosol mass balance on the chemical species in the dry, transition and wet periods and for day and night samples. Mineral fraction = estimated mass fraction due to insoluble inorganic oxides; WSOM = water-soluble organic mass; inorganic ions = water-soluble inorganic ionic material. (a) Dry period; (b) transition period; (c) wet period.
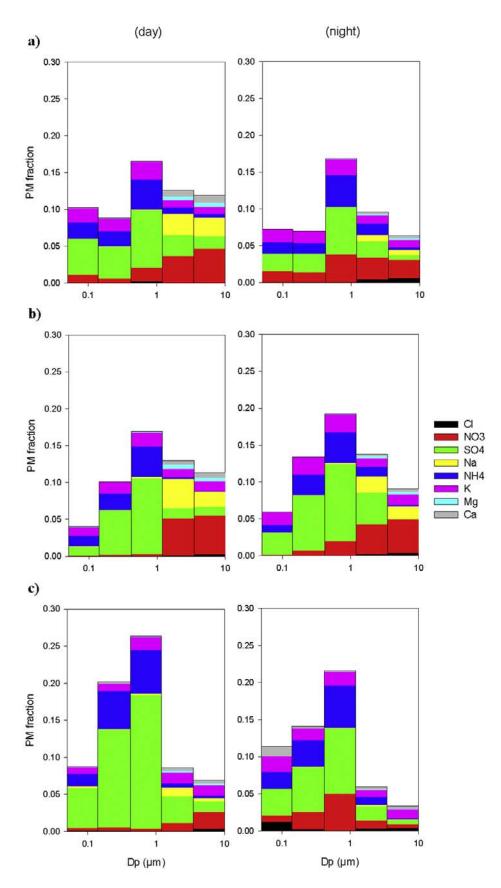
Figure 9. Size-resolved contribution of inorganic ionic species to PM for the dry, transition and wet periods and for day and night samples. (a) Dry period; (b) transition period; (c) wet period.

Table 3. Statistics of Temperature, Relative Humidity, and Solar Radiation

		14–22 Sept	21–29 Oct	31 Oct to 15 Nov
Temperature (°C)	Min	22.4	23.3	22.8
	Max	34.3	34.2	30.8
	Mean	27.9	28.1	25.8
Relative humidity (%)	Min	49	53	66
	Max	98	98	99
	Mean	76	79	87
Solar radiation	Integrated (MJ m^{-2} day^{-1})	18.3	21.6	16.9
	Max (W m^{-2})	782	812	670

nocturnal and diurnal samples, irrespectively of the variations in relative humidity, temperature and oxidizing capacity of the atmosphere, indicating that the carbonaceous particles produced by biomass burning were mainly primary compounds, or at least formed very close to the fires, as also shown by *Guyon et al.* [2005]. The contribution of secondary compounds, like nitrate and sulphates, to PM is minimal. The good agreement between the trend of WSOC and that of potassium ($r^2 = 0.93$) suggests that the polar fraction of particulate organic compounds was also mainly of primary origin or formed during the early ageing of the plumes.

4.1.3. Size-Segregated Inorganic Composition

[43] The conclusions on the relative importance of the various sources of fine PM during dry polluted conditions are not necessarily valid when considering specific size fractions. The evolution of the composition of fine particles in the size ranges 0.05–0.14, 0.14–0.42 and 0.42–1.2 μm of the 5-stage BI is shown in Figure 12. During the initial less polluted conditions, there was a "background" of aerosols characterized by a relatively high amount of sulphate, especially in the 0.42–1.2 μm size range. High concentrations of SO_2, up to several hundreds ppt in the middle to upper troposphere, have been detected over northern São Paulo state (F. Arnold, personal communica-

tion, 2005), most likely deriving from fossil fuel and industrial emissions. This evidence supports the hypothesis of a contribution to the observed "background" sulphate aerosols at the FNS from long-range transport of polluted air masses from distant sources.

[44] After 15 September, the SO_4/PM ratio shows clear minima during the nights, which is correlated with the significant increase in the concentrations of sulphate-poor carbonaceous particles in the nocturnal surface layer after the onset of widespread biomass combustion. As a consequence, organic compounds and potassium became systematically enriched relatively to sulphate at nighttime (Figures 12b and 12c). However, the decrease of sulphate contribution to PM during the night was much more relevant in the finest size intervals (0.05–0.14 and 0.14–0.42 μm) compared to the 0.42–1.2 μm size range.

[45] The figure also shows that the daytime SO_4/PM, SO_4/K and SO_4/WSOC ratios were initially rather constant, but starting on 19 September, after about three days of persistent biomass-burning emissions in a stable atmosphere, they also showed a negative trend, reaching a minimum on 21 September. At that time, the contribution of sulphate to PM was reduced by almost a factor of 2 in the 0.42–1.2 μm range, compared to the initial less polluted conditions. This finding can be explained by a slow accu-
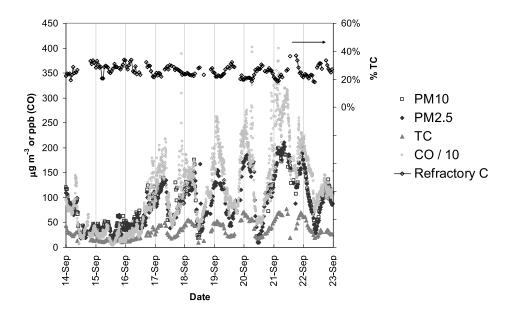

Figure 10. Trends of CO, PM$_{10}$, PM$_{2.5}$ and aerosol TC concentrations determined by high time resolution measurements during the period 14–21 September. The ratio between refractory carbon and TC determined by the carbon monitor is also reported. The horizontal scale is in local time units.
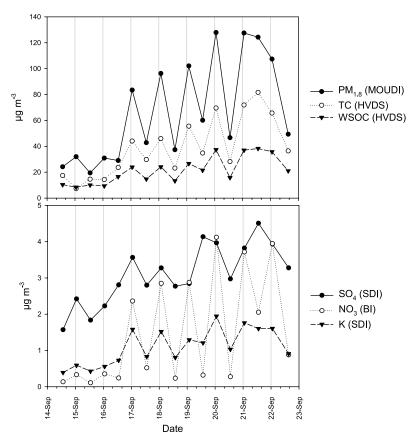
Figure 11. Trends of (a) PM, TC, WSOC and (b) main inorganic species concentrations in the submicrometer fraction of the aerosol in the period 14–21 September. The carbon fractions were determined on HVDS filter samples (PM$_{2.5}$), whereas PM and the inorganic ions concentrations were derived from impactor data integrated over the submicron size range: PM$_{1.8}$, PM$_{1.7}$ and PM$_{1.2}$ for MOUDI, SDI and BI, respectively. The horizontal scale is in local time units.

mulation of sulphate-poor carbonaceous particles produced overnight in the CBL.

[46] In conclusion, the onset of stable dry conditions with consequent accumulation of biomass-burning smoke in the boundary layer *did not* lead to a progressive ageing of the aerosol. On the contrary, it caused a replacement (rapid and almost complete for the finest size range of the aerosol in the nocturnal surface layer; slower and partial for larger particles in the diurnal mixing layer) of the background sulphate aerosols with fresh carbonaceous aerosols produced mainly by smouldering fires.

4.1.4. Size-Segregated Organic Composition

[47] The extensive analyses of the polar organic compounds performed during the SMOCC experiment [*Falkovich et al.*, 2005; *Schkolnik et al.*, 2005; *Decesari et al.*, 2006] allowed the tracing of changes in the aerosol organic composition (Figure 13), analogous to the above observations for inorganic compounds.

[48] The concentrations of the most abundant speciated compounds, e.g., polyhydroxylated compounds (mainly levoglucosan), determined in PM$_{2.5}$ HVDS samples [*Decesari et al.*, 2006], show a clear diurnal variation with enrichment during the night. This is due to the fact that higher levels of levoglucosan and anhydrosugars are emit-

ted for smouldering combustion than for flaming fires [*Schkolnik et al.*, 2005].

[49] Neutral compounds (NC) from IC-UV analysis of BI samples [*Decesari et al.*, 2006] were enriched in WSOC during the night, especially in the smallest size range. The diurnal variations became more pronounced after 16 September, closely following those of polyhydroxylated compounds, suggesting that the processes leading to the production of the anhydrosugars were also responsible for the formation of most of the other nonacidic organic compounds.

[50] The concentrations of polyacidic compounds (PA) also show diurnal variations (but not before 16 September) especially in the finest particles, however, contrary to NC, their contribution to WSOC was higher during daytime. This trend is in agreement with that of high molecular weight (HMW) WSOC determined by EGA analysis on filter samples [*Hoffer et al.*, 2005], and also with the measurements of refractory carbon performed by the carbon monitor. All these measurements point to the same conclusion that the processes leading to the formation of HMW organic material are less efficient during smouldering combustion, mostly occurring overnight. According to laboratory experiments showing that HMW organic compounds can form by oxidation of simple organic molecules by H$_2$O$_2$
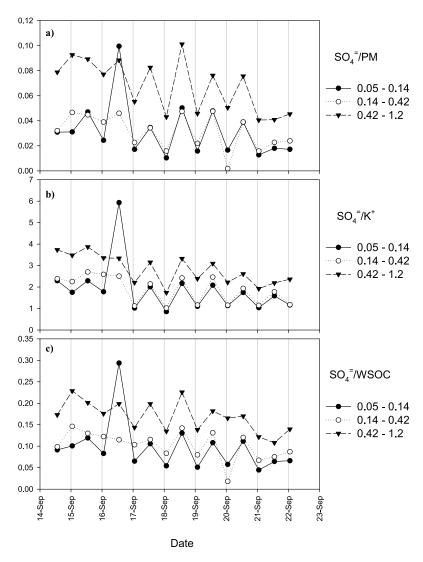
Figure 12. Size-segregated ratios of sulphate to (a) PM, (b) K and (c) WSOC, determined on the 5-stage BI for the period 14−21 September. The submicron size intervals of the BI are reported in the legend: 0.05−0.14, 0.14−0.42, 0.42−1.2 μm. The horizontal scale is in local time units.

in liquid particles [*Gelencsér et al.*, 2003], it was also hypothesized that photochemistry may have played a role in the diurnal variation of WSOC chemical composition [*Hoffer et al.*, 2005].

[51] In summary, when the meteorological conditions were stable, the enhanced emission of primary TC and WSOC from fires triggered the sharp increase in fine PM concentrations in Rondônia. However, the chemical composition of the carbonaceous material was not constant with time and not homogenous over the aerosol size spectrum. In particular, fresh organic material, characterized by a high content of levoglucosan and other hydroxylated compounds, was emitted overnight by smouldering fires. These freshly produced compounds were superimposed (especially in the finest size ranges) on particles enriched in high molecular weight, thermally refractory organic compounds, which had been initially dominant in the daytime boundary layer. The enrichment of high molecular weight organic compounds in the daytime CBL aerosol

could be due to either strong emission from flaming fires or to chemical ageing of the aerosol.

4.2. Subperiod 2 (21−29 October 2002)

[52] During this period, the only precipitation event was on 21 October, when a rainfall (12.3 mm) occurred in the early evening. However, it should be emphasized that from 17 until 21 October, heavy rainfall took place (total precipitation amounted to 100 mm over 4 days) and the soil was wet. Cloudy conditions characterized by a reduced height of the boundary layer (1000−1300 m) were encountered on 21−23 and 25−26 October. Toward the end of the period, clear sky conditions prevailed and the height of the mixing layer reached 1500 m.

[53] Extremes of temperature ranged between 22−24°C and 33−35°C. The RH values ranged between 50−60% during midafternoon and 95−100% after sunset. No large-scale meteorological phenomena influenced the weather at the site. The rainfall was mostly due to local convection and sparse isolated cells.
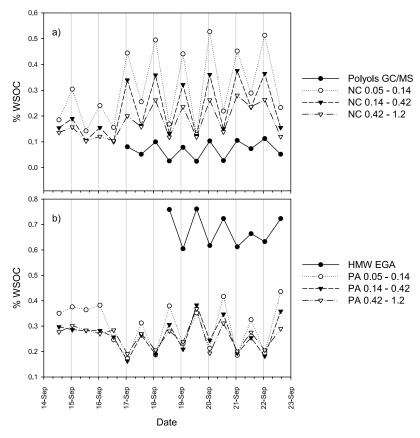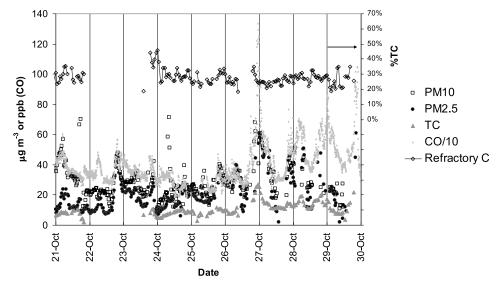
Figure 13. Size-segregated ratios of classes of organic compounds to WSOC for the period 14−21 September: (a) polyhydroxylated compounds (polyols) determined by GC/MS analysis of HVDS PM$_{2.5}$ filters; neutral compounds (NC) determined by IC-UV analysis of BI samples; (b) high molecular weight (HMW) WSOC determined by evolved gas analysis (EGA) on HVDS PM$_{2.5}$ filters; polyacids (PA) determined by IC-UV analysis of BI samples. The submicron size intervals of the BI are reported in the legend: 0.05−0.14, 0.14−0.42, 0.42−1.2 μm. The horizontal scale is in local time units.

Figure 14. Trends of CO, PM$_{10}$, PM$_{2.5}$ and aerosol TC concentrations determined by high time resolution measurements during the period 21−30 October. The ratio between refractory carbon and TC determined by the carbon monitor is also reported. The horizontal scale is in local time units.

4.2.1. High Time Resolution Aerosol Measurements

[54] The trends of CO and PM_{10} and $PM_{2.5}$ from TEOM (Figure 14) show rather irregular profiles during the first part of the period, from 20 to 24 October, and large diurnal oscillations over the subsequent days, displaying the same dynamics already observed in the dry period: as soon as the meteorological conditions became stable, the burning activities in the region resumed, leading to a steep increase in the concentrations of CO and PM in the shallow nocturnal surface layer. The increase in daytime concentrations was less marked compared to nighttime, because the rise in the height of the mixing layer (reaching 1500 m by the end of the period) compensated for the stronger emissions from new fires. The close correlation between the profile of CO concentration and that of PM concentration characteristic of the dry period does not exist in this case. The CO concentrations varied between 300 and 500 ppb from 21 to 26 October, reaching 700 ppb during nighttime of the subsequent days. The PM_{10} and $PM_{2.5}$ concentration maxima usually corresponded to those of CO, but TEOM profiles indicate that aerosol concentrations were much more variable than those of CO throughout the period.

[55] Unlike during the dry period, in the transition period the same straight correlation between the time series of $PM_{2.5}$ and PM_{10} is not observed. The PM_{10} was often significantly higher than $PM_{2.5}$, up to a factor of two, on 21–23 October, while the two trends overlap quite well during the following period characterized by drier conditions. Conversely, there is always a good agreement between the trends of $PM_{2.5}$ and TC from the carbon monitor, with an average TC/PM ratio of about 0.44. These data indicate that during the transition phase, submicrometer particles were still dominated by carbonaceous aerosols emitted by biomass burning. However, the levels of PM_{10} concentrations from TEOM were rather constant throughout the period, because the lower concentrations of biomass-burning particles during the first days characterized by relatively wet conditions were compensated by higher concentrations of coarse-mode particles, possibly due to suspension of particles by winds associated with the passage of storms.

4.2.2. Time-Integrated Aerosol Measurements

[56] Sampling with filters and impactors during the transition period was performed over time intervals of approximately 24 hours. Samples of filter devices, DLPI, BI and 11-stage MOUDI were collected in parallel during two consecutive nights or days. The concentrations of PM_{10}, $PM_{2.5}$, TC and WSOC determined on filter samples show an increase of a factor of two in both daytime and nighttime concentrations throughout the period (Figure 15a). This indicates that also during the transition period the submicrometer aerosols were mainly carbonaceous particles from biomass burning. It should be noted that the rise in the pyrogenic particle concentration after the end of a rain event was modest in the transition period compared to the dry period, when $PM_{2.5}$ and TC concentrations increased by a factor of four in only two days without precipitation.

[57] The analysis of the major inorganic ions in submicron aerosol from integrated impactor samples shows that sulphate dominated the inorganic composition throughout the period (Figure 15b). Particulate nitrate was also observed in the nocturnal samples but, contrary to the dry period, the concentrations stayed well below those of sulphate. The ratios K/SO_4 were also on average lower in the transition period compared to the dry period, indicating a higher proportion of ionic material formed by secondary processes, which is consistent with the more aged character of the combustion products as indicated by the CO profiles. In fact, SO_2 levels in the transition period, determined by the wet annular denuder measurements, were about 100–200 ppb [*Trebs et al.*, 2004], i.e., 1/3–1/2 of those observed in the 14–21 September period. This explains why the concentrations of particulate sulphate in $PM_{1.7}$ (from integrated SDI stages) during the transition period (1 to 2 μg m^{-3}) were only half of those found for the dry period, despite a decrease of 4–5 times in $PM_{2.5}$ and TC. Apparently, relatively high background concentrations of sulphur dioxide ensured a stable reservoir of sulphate aerosols, which became important, compared to the other aerosol constituents (i.e., TC, K salts and nitrate) outside the period of more intense fire activity. This offers an explanation for the generally high contribution of sulphate to the aerosol mass budget shown in Figure 9. Actually, the conversion of sulphur dioxide to sulphate is not likely to be constant during the experiment, because of the various ambient conditions influencing the photochemical activity and the in-cloud oxidation processes. During the period considered here (21–29 October), the daytime concentrations of sulphate increased by a factor of two from 20–21 October to 26–27 October. Conversely, the nighttime concentrations increased by only 25% over the period. This suggests that the clear-sky conditions encountered after 24 October increased the production of sulphate in daytime compared to that at nighttime. By contrast, the effect of cloud processing in sulphate formation cannot be clearly evidenced.

4.2.3. Size-Segregated Inorganic Composition

[58] The changes in the size-segregated SO_4/WSOC and SO_4/K ratios in the period 20–29 October are shown in Figures 16a and 16b. Data were obtained from BI samples. Since each sample was collected over two 12-hour time intervals for two consecutive nights or days, the diurnal variations in the chemical composition could not be followed in a continuous way. However, Figures 16a and 16b clearly shows that systematic differences between the diurnal and nocturnal compositions were encountered in this period, suggesting that the processes responsible for aerosol formation in the transition period were similar to those active in the dry period. The enrichment of potassium and organics relative to sulphate in submicron particles during the night is clearly seen throughout the period. Such enrichment is more significant in the smallest particles (a factor of two in the 0.05–0.14 μm size range). This indicates that primary compounds from smouldering sources during nighttime affect the composition of the aerosol mainly in the lowest size range. Similar results were obtained for the period of most intense burning (see Figure 12). However, in the dry period, the nocturnal enrichment of potassium and organics relative to sulphate was larger by a factor of two for particles up to 0.42 μm size range.

[59] In conclusion, changes in the size-segregated aerosol composition due to the diurnal evolution of the pyrogenic sources and of the boundary layer structure were found throughout the period considered here, indicating that the
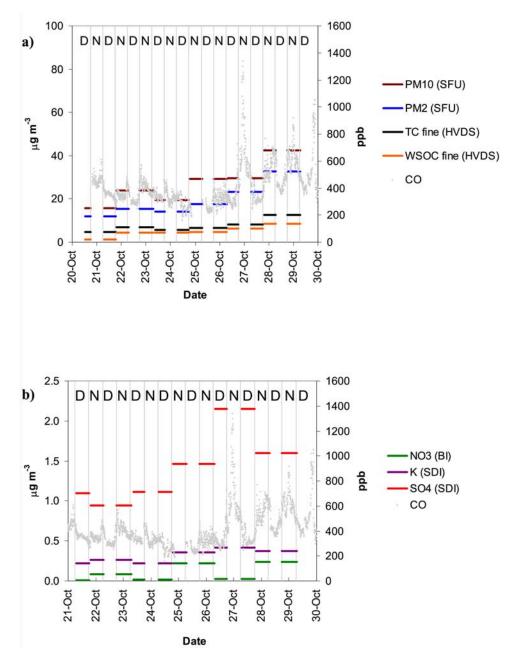
Figure 15. (a) Concentrations of PM_{10}, PM_2, TC and WSOC determined in filter samples in the period 21–30 October. b) Concentrations of the main inorganic ions from impactor data integrated over the submicron size range, in the same period: $PM_{1.7}$ and $PM_{1.2}$ for SDI and BI, respectively. The CO concentration profile is also shown in the figure. 'D' and 'N' refer to day and night. The horizontal scale is in local time units.

aerosol composition was affected by relatively fresh smoke particles. The dynamics of aerosol formation and transformation by such emissions are the same as those identified in the dry period. However, primary biomass-burning compounds, traced by low SO_4/K ratios, affected the composition of aerosol particles with diameter larger than 0.14 μm to a lesser extent in the transition period compared to the dry period. Furthermore, the sulphate contribution in the size range 0.14–1.2 μm shows no trend during the transition period, indicating that there is no accumulation of fresh aerosol particles produced overnight in the diurnal CBL. Such relatively stable aged population of sulphate-rich

aerosol particles can be responsible for the background concentrations of $PM_{2.5}$ particles as seen in the TEOM time trends.

4.2.4. Size-Segregated Organic Composition

[60] Figures 17a and 17b provides insights into the changes in the chemical composition of the polar fraction of aerosol OC (WSOC). The relative contributions of the chemical classes determined by IC-UV analysis of the BI samples are shown in the figure, together with the HMW-WSOC from EGA analysis and the poly hydroxylated compounds (mainly anhydrosugars) from GC/MS. As in the dry period, neutral compounds (NC) and anhydrosugars
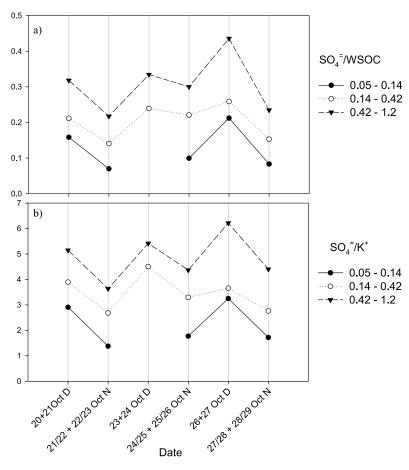
Figure 16. Size-segregated ratios of sulphate to (a) WSOC and (b) K, determined on the 5-stage BI for the period 21–30 October. The size intervals of the BI are reported in the legend: 0.05–0.14, 0.14–0.42, 0.42–1.2, 1.2–3.5, 3.5–10 μm. The horizontal scale is in local time units.

are enriched compared to total WSOC in the nocturnal samples in all size ranges (Figure 17a). On the other hand, polyacids (PA) do not show any clear diurnal maxima, but there is a slight enrichment in WSOC in the 0.14–0.42 μm size range. The HMW fraction of WSOC by EGA analysis still shows a diurnal variation, which is much less pronounced than during the dry period (Figure 17b). These findings are in agreement with the measurements of the carbon monitor, which showed a rather constant fraction of refractory carbon throughout the period. According to *Hoffer et al.* [2005], HMW organic compounds are formed continuously during the ageing of the aerosol through polymerization of aromatic acids promoted by sunlight. Following this hypothesis, the higher proportion of HMW compounds with less diurnal variations in the transition period compared to the dry period, should be attributed to the more aged character of the aerosol. However, the patterns in the NC composition indicate that some distinct evolution processes in the WSOC composition linked to the biomass-burning activity of the dry period are still active in the transition period.

4.3. Subperiod 3 (31 October to 15 November 2002)

[61] Meteorological conditions in this period were very similar to the transition case. Extremes of temperature ranged between 22–23°C for the lowest values and 30–31°C for the highest values. The RH values ranged

between 65–70% during midafternoon and 95–100% near sunrise. The numerous rain events during this period, with a total of 50.5 mm of rain in the first 10 days of November reduced the amount of solar radiation reaching the surface. No radiosoundings are available for the period.

[62] At the beginning of November, only 24 fire spots were reported in Rondônia (Figure 2b) for the first 15 days, as measured by NOAA-14. However, fires were still active in the nearby Mato Grosso state (Figure 1c), with the occurrence of 497 fires in the period November 1–15.

4.3.1. High Time Resolution Aerosol Measurements

[63] The trend of CO concentration shows a slight decrease from the last, relatively polluted, days of October, down to ∼200 ppb, with no further change during the first two weeks of November (Figure 18). This indicates that the products of combustion with relatively long lifetime were well mixed in the boundary layer, which can be explained by a longer-range transport. Therefore at the onset of the wet season, the distributions of the pyrogenic sources was completely different from that of the middle dry season, when the massive emissions of fresh smoke during nighttime triggered the rise in CO concentrations up to 3000 ppb.

[64] Data from TEOM and the carbon monitor are available for this period only until 3 November. The concentrations of PM$_{2.5}$, PM$_{10}$ and TC show irregular variations, with no trends and no apparent correlation with the profile
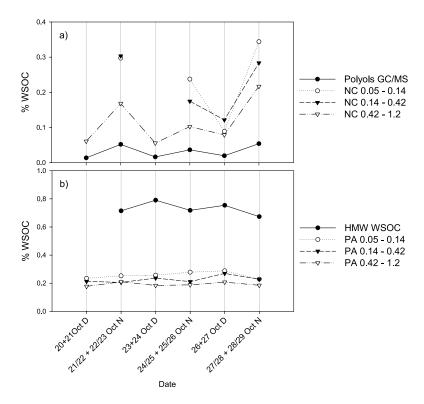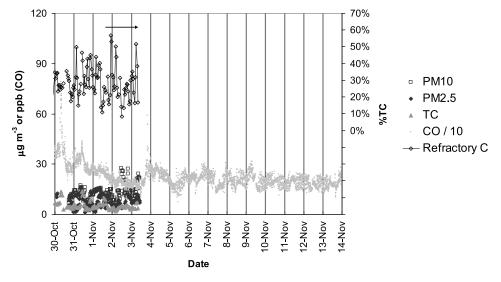
Figure 17. Size-segregated ratios of classes of organic compounds to WSOC for the period 21–30 October: (a) polyhydroxylated compounds (polyols) determined by GC/MS analysis of HVDS PM$_{2.5}$ filters; neutral compounds (NC) determined by IC-UV analysis of BI samples; (b) high molecular weight (HMW) WSOC determined by evolved gas analysis (EGA) on HVDS PM$_{2.5}$ filters; polyacids (PA) determined by IC-UV analysis of BI samples. The submicron size intervals of the BI are reported in the legend: $0.05-0.14$, $0.14-0.42$, $0.42-1.2$ μm. The horizontal scale is in local time units.

Figure 18. Trends of CO, PM$_{10}$, PM$_{2.5}$ and aerosol TC concentrations determined by high time resolution measurements during the period 30 October to 14 November. The ratio between refractory carbon and TC determined by the carbon monitor is also reported. Measurements of PM$_{10}$, PM$_{2.5}$ and TC stopped on 31 October. The horizontal scale is in local time units.
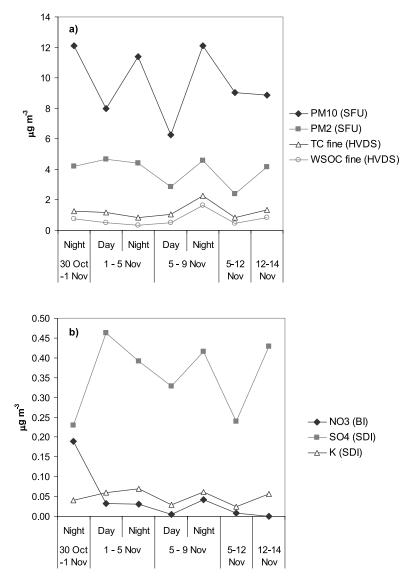
Figure 19. Concentrations of (a) PM_{10}, PM_2, and of TC and WSOC in the fine fraction of the aerosol determined in filter samples, and (b) concentrations of main inorganic ions from impactor data integrated over the submicron size range ($PM_{1.7}$ and $PM_{1.2}$ for SDI and BI, respectively), in the period 30 October to 14 November. The horizontal scale is in local time units.

of CO. The ratio between refractory carbon and TC show no diurnal variation either.

4.3.2. Time-Integrated Aerosol Measurements

[65] Only a small number of samples could be collected on filters and impactors, because the sampling time generally had to be extended to ~48 h to allow sufficiently loaded samples. Only during the last two days of October, when the higher aerosol concentrations encountered at the end of the transition period was not completely abated by the enhanced precipitation, was one set of 24 h samples collected over two consecutive nights. Then, from 1 to 5 November, sampling was performed separately for the night and the day, leading to two sets of 48 h samples. Similarly, another couple of sample sets (one diurnal and one nocturnal) was collected between 5 and 9 November. Finally, sampling was also performed from 10 to 12 November and from 12 to 14 November with no distinction between day and night.

[66] The average PM concentrations in the fine fraction (PM_2 from SFU samples) were only $3-4$ μg m^{-3} during the wet period with no apparent trend (Figure 19a). Coarse-mode particle concentration reached $4-8$ μg m^{-3} with little or no trend. Since the samples were collected over long time intervals, it is possible that the average concentrations were driven by short episodes of relatively high concentrations. TC and WSOC in $PM_{2.5}$ exhibit similar trends and, after 5 November the TC/PM_2 ratios are about 0.40, as in the transition period, indicating that fine particles are essentially carbonaceous (see section 3.5). Somewhat lower ratios are characteristic of the first days of November.

[67] Concentrations of the main aerosol inorganic compounds, integrated over the submicron size range, were obtained from impactor measurements with DLPI and SDI (Figure 19b). Except for the first sample, showing an unusually high NO_3/SO_4 ratio, the concentrations of potassium, nitrate and sulphate followed a similar trend. How-
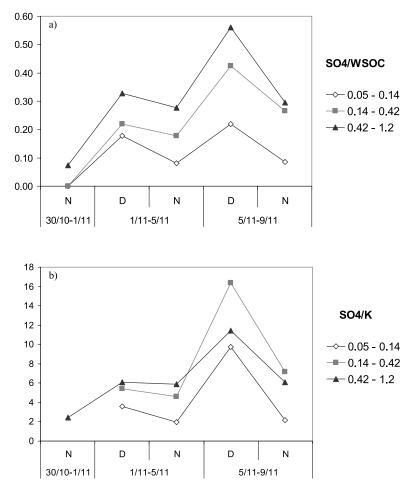
Figure 20. Size-segregated ratios of sulphate to (a) WSOC and (b) K, determined on the 5-stage BI for the period 30 October to 14 November. The size intervals of the BI are reported in the legend: 0.05–0.14, 0.14–0.42, 0.42–1.2, 1.2–3.5, 3.5–10 μm. The horizontal scale is in local time units.

ever, the nighttime concentrations of nitrate changed by a factor of ten with respect to daytime, those of potassium by a factor of two, while the lowest variations were observed in the sulphate concentration. The maxima in the PM_2 mass, TC and inorganic ions concentrations appear to be connected with episodes of very high concentrations of potassium and especially nitrate in the fine aerosol fraction. Apparently, biomass-burning emissions from local fires caused an increase in the PM_2 mass, TC and potassium concentrations, which was relevant in the period 5–9 November, while most (60–90%) of sulphate-rich particles were likely associated with the background aerosol.

4.3.3. Size-Segregated Composition

[68] The size-segregated data from the BI samples were obtained for the period 29 October to 9 November. Since no time trends for the organic compounds were obtained, only the inorganic composition is discussed here (Figures 20a and 20b). Sulphate contribution increased compared to WSOC and K in all submicrometer size ranges, especially in daytime conditions, with a trend which is opposite to the one observed during the peak of the biomass-burning season (see Figure 12). As previously observed, during the transition period low SO_4/WSOC and SO_4/K values are found in the lowest size range (0.05–0.14 μm) for

nocturnal samples, whereas the diurnal variations of these ratios for larger particles are smaller. Such findings indicate that during the period under consideration, even with almost background conditions, the smoke significantly affected the composition of the aerosol especially in the finest size range (<0.14 μm) during the night. The SO_4/WSOC and SO_4/K ratios observed in daytime for particles with diameter of 0.42–1.2 μm in the wet period were three to four times higher than in the dry period. Therefore during the wet period, the accumulation of sulphate-rich accumulation-mode particles in the boundary layer became the dominant process. Our hypothesis concerning the formation of a stable background of fine aerosol particles from aged combustion products is supported by the CO time series and the relative high content of sulphate in these particles.

[69] Nonetheless, the contribution of biogenic sources to the organic fraction of background particles should not be underestimated. A relatively constant K/WSOC ratio of ~0.05, characteristic of biomass-burning emissions [*Graham et al.*, 2002], was found in all size ranges throughout the campaign until the end of the transition period (Figure 21). However, this ratio is significantly lower during the wet period in the case of the fine aerosol fraction. Such decrease in the submicron size range hint at sources of
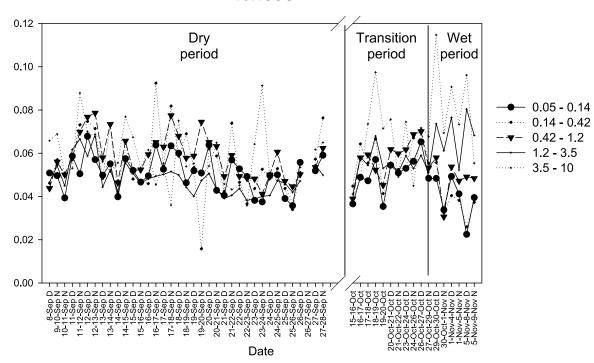
Figure 21. Potassium versus WSOC (K/WSOC) ratio determined for 5-stage BI samples. The BI was not deployed from 29 September to 14 October. The size intervals of the BI are reported in the legend: 0.05–0.14, 0.14–0.42, 0.42–1.2, 1.2–3.5, 3.5–10 μm.

OC other than biomass burning, thus possible biogenic emissions. In conclusion, there is evidence that biogenic organic compounds contributed significantly to fine PM together with aged pyrogenic compounds (both OC and ammonium sulphate) in the wet period.

5. Conclusions

[70] The aerosol characterization experiment performed during the LBA-SMOCC field campaign provided a unique data set of size-resolved chemical composition of boundary layer aerosol over the Amazon Basin during the dry-to-wet season transition. Although sampling was performed at a single station located in a pasture site, the data on aerosol composition and concentration are representative also for the neighboring areas [*Artaxo et al.*, 2002], since aerosol loads in the boundary layer were mainly controlled by burning activities extending over large areas in the states of Rondônia, Mato Grosso, and other upwind states in the arc of deforestation, and (with respect to removal processes) by large-scale convective systems (M. A. F. Silva Dias, in preparation, 2006). Substantial improvements were made in the characterization of the size distributions of inorganic and organic components of the aerosol, owing to the systematic deployment of multistage impactor-based sampling techniques. In this way, the size-resolved particulate matter was apportioned into its main organic and inorganic chemical constituents. On the one hand, our findings provide confirmation of the outcomes of previous LBA experiments, showing that the supermicron fraction of the aerosol is composed mainly of primary particles of crustal or biological origin, whereas submicron particles are produced in

high concentrations only during the biomass-burning period, and are mainly composed of organic material with ∼10% of soluble inorganic salts, including sulphate as the major anion. On the other hand, evidence was found that inorganic (e.g., nitrates) and organic (e.g., levoglucosan) compounds originating from biomass burning exist also in the coarse particles, a fact that was particularly evident in the wet period of the experiment. Furthermore, the occurrence of methyltetrols in the fine aerosol fraction in all periods indicates that a natural background of secondary organic aerosols produced by isoprene oxidation [*Claeys et al.*, 2004a] affected the composition of submicrometer particles, and their contribution was highest during the wet period. Size-segregated data indicate that the chemical composition was not homogeneous with aerosol size. In particular, inorganic ions were enriched in large accumulation-mode particles, where they accounted for up to 20% of aerosol mass, whereas lower proportions (usually below 10%) were encountered in the finest size fractions. Previous experiments, relying on elemental (PIXE) analysis, did not provide measurements of the N-containing compounds, i.e., ammonium and nitrate, which, during LBA-SMOCC, were found to account for 20–50% of the inorganic water-soluble mass. In particular, our data show that ammonium (not potassium) was the most abundant cation in all periods of the campaign and in all size fractions, indicating that condensation of inorganic gaseous compounds normally occurred on smoke particles. Nitrate size distributions varied in shape and size according to season and day/night conditions. This can be interpreted as the different effects of acidity/alkalinity of the particles, surface size distribution of the preexisting aerosol population and especially ambient conditions (T, RH) on nitric acid condensation/evaporation

rates. Nitrate was as abundant as sulphate at nighttime in the dry period, whereas sulphates dominated the inorganic composition in the wet period. The WSOC represent the major fraction of the aerosol OC in the submicron size range throughout the experiment, in agreement with results from the previous LBA campaign, which were obtained from samples collected in the dry and transition periods in 1999 [*Mayol-Bracero et al.*, 2002]. In contrast, coarse aerosol particles are characterized by a large fraction of insoluble carbonaceous material of primary biogenic origin. These coarse-mode primary biogenic particles were present throughout the experiment. Some of these particles could act as "giant CCN" and contribute significantly to cloud formation [*McFiggans et al.*, 2006].

[71] Size-resolved average aerosol chemical compositions were obtained for the dry, transition and wet periods. However, significant variations in the aerosol composition and concentrations were observed within each period. Such variations can be classified into two categories:

[72] 1. Diurnal variations, caused by the diurnal cycle of the boundary layer, the marked difference in ambient conditions (T and RH) between day and night, and the different prevalent combustion phase active during day (flaming) or night (smouldering). The magnitude of variation in all these factors is higher in the dry period, leading to large variations in the aerosol chemical composition and oscillating trends of concentration. Typically, very high concentrations of freshly emitted smoke particles, rich in organic material (with anhydrosugars as markers) and nitrate but poor in sulphate, are found at nighttime. By contrast, lower concentrations due to efficient mixing of the boundary layer were encountered in daytime, and the aerosol composition was characterized by a high content of refractory carbon, humic-like material and sulphates.

[73] 2. Day-to-day variations, due to alternating phases of relatively wet and dry conditions. The development of widespread convection in the region was sporadic in the dry period but its frequency increased toward the end of the experiment. During the dry period, Rondônia experienced about seven days with no intense precipitation events (aside from local convection), so that biomass-burning particles emitted from a number of fires in the region were able to accumulate in the boundary layer. Data from chemical analyses show that the aerosols in the transition and wet periods exhibit a more aged character compared to the dry period, showing a higher sulphate/potassium and sulphate/WSOC ratios. Finally, in the wet period, a lower K/WSOC ratio was found in the submicron fraction of the aerosol, suggesting that sources of organic material other than biomass burning significantly contributed to the aerosol OC at that time.

[74] The analysis of the impactor samples collected during the LBA-SMOCC experiment has provided a comprehensive data set of aerosol size-resolved chemical composition over areas affected by biomass burning. Compared to previous studies conducted both in the same area [*Artaxo et al.*, 2002] and other regions [*Ruellan et al.*, 1999; *Formenti et al.*, 2003], the LBA-SMOCC aerosol characterization experiment was uniquely comprehensive with respect to the chemical determinations and the coverage of aerosol climatology (i.e., seasonal trends and diurnal variations). The chemical data set provided by the SMOCC field experiment was used to characterize the aerosol hygroscopic properties and ability to act as cloud condensation nuclei (CCN) [*Mircea et al.*, 2005]. The high content of WSOC in biomass-burning particles was found to be responsible for the observed low hygroscopic growth factors and for the measured CCN spectra characterized by a steady increase in the CCN ability with supersaturation [*Andreae et al.*, 2004; *Mircea et al.*, 2005; *Rissler et al.*, 2006]. Such studies have shown that the changes in the aerosol chemical composition with particle size are relevant to the hygroscopic properties of the aerosol. Indeed, size distribution information indicates that the relative amount of inorganic ionic material versus the organic compounds is almost half for particles of diameter of 100 nm compared to larger particles of 1 μm size. Moreover, potassium salts were enriched in small (Dp $\sim$ 100 nm) biomass-burning particles, whereas larger (Dp $\sim$ 1 μm) particles contained larger amounts of more soluble ammonium salts. Such variations in the chemical composition with particle size, which are important in determining the interaction of aerosol with water in the atmosphere (hygroscopic growth and cloud droplet formation), were clearly measured by the multistage impactors, whereas they eluded the filter-based sampling techniques, which have been previously employed. The present work within the LBA-SMOCC experiment represents, to our knowledge, the most extensive characterization of size-segregated biomass-burning aerosol to date. Given the importance of biomass burning for the global atmosphere and in order to provide reliable input data and parameterizations to models, it would be highly important that a similar experimental approach is used in other regions of the world affected by extensive biomass burning (e.g., Africa, Indonesia, Australia, Southern Europe) to evaluate similarities and differences in physical and chemical properties of biomass-burning aerosol at the global level. Improved sampling/analytical techniques should also be implemented which allow airborne aerosol measurements of a similar complexity as the ground-level measurements presented here.

References

Andreae, M. O., et al. (1998), Airborne studies of aerosol emissions from savanna fires in southern Africa: 2. Aerosol chemical composition, *J. Geophys. Res.*, *103*, 32,119–32,128.

Andreae, M. O., W. Elbert, R. Gabriel, D. W. Johnson, S. Osborne, and R. Wood (2000), Soluble ion chemistry of the atmospheric aerosol and SO2 concentrations over the eastern North Atlantic during ACE-2, *Tellus, Ser. B*, *52*, 1066–1087.

Andreae, M. O., et al. (2002), Biogeochemical cycling of carbon, water, energy, trace gases, and aerosols in Amazonia: The LBA-EUSTACH experiments, *J. Geophys. Res.*, *107*(D20), 8066, doi:10.1029/2001JD000524.

Andreae, M. O., D. Rosenfeld, P. Artaxo, A. A. Costa, G. P. Frank, K. M. Longo, and M. A. F. Silva-Dias (2004), Smoking rain clouds over the Amazon, *Science*, *303*, 1337–1342.

Artaxo, P., and H. C. Hansson (1995), Size distribution of biogenic aerosol particles from the Amazon basin, *Atmos. Environ.*, *29*(3), 393–402.

Artaxo, P., E. T. Fernandez, J. V. Martins, M. A. Yamasoe, P. V. Hobbs, W. Maenhaut, K. M. Longo, and A. Castanho (1998), Large scale aerosol source apportionment in Amazonia, *J. Geophys. Res.*, *103*, 31,837–31,848.

Artaxo, P., R. C. de Campos, E. T. Fernandez, J. V. Martins, Z. Xiao, O. Lindqvist, M. T. Fernandez-Jimenez, and W. Maenhaut (2000), Large scale mercury and trace element measurements in the Amazon Basin, *Atmos. Environ.*, *34*, 4085–4096.

Artaxo, P., J. Vanderlei Martins, M. A. Yamasoe, A. S. Procopio, T. M. Pauliquevis, M. O. Andreae, P. Guyon, L. V. Gatti, and A. M. Cordova Leal (2002), Physical and chemical properties of aerosols in the wet and dry seasons in Rondônia, Amazonia, *J. Geophys. Res.*, *107*(D20), 8081, doi:10.1029/2001JD000666.

Chand, D., P. Guyon, P. Artaxo, O. Schmid, G. P. Frank, L. V. Rizzo, O. L. Mayol-Bracero, L. V. Gatti, and M. O. Andreae (2006), Optical and physical properties of aerosols in the boundary layer and free troposphere over the Amazon Basin during the biomass burning season, *Atmos. Chem. Phys.*, *6*, 2911–2925.

Claeys, M., et al. (2004a), Formation of secondary organic aerosols through photooxidation of isoprene, *Science*, *303*, 1173–1176.

Claeys, M., W. Wang, A. C. Ion, I. Kourtchev, A. Gelencsér, and W. Maenhaut (2004b), Formation of secondary organic aerosols from isoprene and its gas-phase oxidation products through reaction with hydrogen peroxide, *Atmos. Environ.*, *38*, 4093–4098.

Decesari, S., et al. (2006), Characterization of the organic composition of aerosols from Rondônia, Brazil, during the LBA-SMOCC 2002 experiment and its representation through model compounds, *Atmos. Chem. Phys.*, *6*, 375–402.

Falkovich, A. H., E. R. Graber, G. Schkolnik, Y. Rudich, W. Maenhaut, and P. Artaxo (2005), Low molecular weight organic acids in aerosol particles from Rondônia, Brazil, during the biomass burning, transition and wet periods, *Atmos. Chem. Phys.*, *5*, 781–797.

Ferreira da Costa, R., J. R. P. Feitosa, G. Fisch, S. S. Souza, and C. A. Nobre (1998), Variabilidade diária da precipitação em regiões de floresta e pastagem na Amazônia, *Acta Amazônica*, *28*(4), 395–408.

Formenti, P., W. Elbert, W. Maenhaut, J. Haywood, S. Osborne, and M. O. Andreae (2003), Inorganic and carbonaceous aerosols during the Southern African Regional Science Initiative (SAFARI 2000) experiment: Chemical characteristics, physical properties, and emission data for smoke from African biomass burning, *J. Geophys. Res.*, *108*(D13), 8488, doi:10.1029/2002JD002408.

Freitas, S., R. M. A. F. Silva Dias, P. L. Silva Dias, K. M. Longo, P. Artaxo, M. O. Andreae, and H. Fischer (2000), A convective kinematic trajectory technique for low resolution atmospheric models, *J. Geophys. Res.*, *105*(D19), 24,375–24,386.

Gabriel, R., O. L. Mayol-Bracero, and M. O. Andreae (2002), Chemical characterization of submicron aerosol collected over the Indian Ocean, *J. Geophys. Res.*, *107*(D19), 8005, doi:10.1029/2000JD000034.

Gao, S., D. A. Hegg, P. V. Hobbs, T. W. Kirchstetter, B. I. Magi, and M. Sadilek (2003), Water-soluble organic components in aerosols associated with savanna fires in southern Africa: Identification, evolution, and distribution, *J. Geophys. Res.*, *108*(D13), 8491, doi:10.1029/2002JD002324.

Gelencsér, A., A. Hoffer, G. Kiss, E. Tombácz, R. Kurdi, and L. Bencze (2003), In-situ formation of light-absorbing organic matter in cloud water, *J. Atmos. Chem.*, *45*, 25–33.

Graham, B., O. L. Mayol-Bracero, P. Guyon, G. C. Roberts, S. Decesari, M. C. Facchini, P. Artaxo, W. Maenhaut, P. Köll, and M. O. Andreae (2002), Water-soluble organic compounds in biomass burning aerosols over Amazonia: 1. Characterization by NMR and GC/MS, *J. Geophys. Res.*, *107*(D20), 8047, doi:10.1029/2001JD000336.

Graham, B., P. Guyon, P. E. Taylor, P. Artaxo, W. Maenhaut, M. M. Glovsky, R. C. Flagan, and M. O. Andreae (2003), Organic compounds present in the natural Amazonian aerosol: Characterization by gas chromatography-mass spectrometry, *J. Geophys. Res.*, *108*(D24), 4766, doi:10.1029/2003JD003990.

Guyon, P., B. Graham, G. C. Roberts, O. L. Mayol-Bracero, W. Maenhaut, P. Artaxo, and M. O. Andreae (2003), In-canopy gradients, composition, sources, and optical properties of aerosol over the Amazon forest, *J. Geophys. Res.*, *108*(D18), 4591, doi:10.1029/2003JD003465.

Guyon, P., W. Maenhaut, M. Blazso, S. Janitsek, A. Gelencser, P. Artaxo, and M. O. Andreae (2004a), Study of tropical organic aerosol by thermally assisted alkylation-gas chromatography mass spectrometry, *J. Anal. Appl. Pyrolysis*, *71*(2), 1027–1029.

Guyon, P., B. Graham, G. C. Roberts, O. L. Mayol-Bracero, W. Maenhaut, P. Artaxo, and M. O. Andreae (2004b), Sources of optically active aerosol particles over the Amazon forest, *Atmos. Environ.*, *38*, 1039–1051.

Guyon, P., et al. (2005), Airborne measurements of trace gases and aerosol particle emissions from biomass burning in Amazonia, *Atmos. Chem. Phys.*, *5*, 2989–3002.

Herrmann, H. (2003), Kinetics of aqueous phase reactions relevant for atmospheric chemistry, *Chem. Rev.*, *103*, 4691–4716.

Hoffer, A., A. Gelencsér, M. Blazsó, P. Guyon, P. Artaxo, and M. O. Andreae (2005), Chemical transformations in organic aerosol from biomass burning, *Atmos. Chem. Phys. Discuss.*, *5*, 8027–8054.

Kawamura, K., R. Semppéré, Y. Imai, Y. Fujii, and M. Hayashi (1996), Water-soluble dicarboxylic acids and related compounds in Antarctic aerosols, *J. Geophys. Res.*, *101*(D13), 18,721–18,728.

Maenhaut, W., R. Hillamo, T. Mäkelä, J.-L. Jaffrezo, M. H. Bergin, and C. I. Davidson (1996), A new cascade impactor for aerosol sampling with subsequent PIXE analysis, *Nucl. Instr. Meth. Phys. Res., Sec. B*, *109/110*, 482–487.

Maenhaut, W., J. Schwarz, J. Cafmeyer, and X. Chi (2002), Aerosol chemical mass closure during the EUROTRAC-2 AEROSOL Intercomparison 2000, *Nucl. Instr. Meth. Phys. Res., Sec. B*, *189*, 233–237.

Maenhaut, W., N. Raes, J. Cafmeyer, and P. Artaxo (2004), Study of elemental mass size distributions in Amazonia during the LBA/CLAIRE/SMOCC-2002 campaign, paper presented at the 10th International Conference on Particle-Induced X-ray Emission and Its Analytical Applications, Jozef Stefan Institute, Portoro, Slovenia, 4–8 June.

Matta, E., M. C. Facchini, S. Decesari, M. Mircea, F. Cavalli, S. Fuzzi, J-.P. Putaud, and A. Dell'Acqua (2003), Mass closure on the chemical species in size-segregated atmospheric aerosol collected in a urban area of the Po Valley, Italy, *Atmos. Chem. Phys.*, *3*, 623–637.

Mayol-Bracero, O. L., P. Guyon, B. Graham, G. C. Roberts, M. O. Andreae, S. Decesari, M. C. Facchini, S. Fuzzi, and P. Artaxo (2002), Water-soluble organic compounds in biomass burning aerosols over Amazonia: 2. Apportionment of the chemical composition and importance of the polyacidic fraction, *J. Geophys. Res.*, *107*(D20), 8091, doi:10.1029/2001JD000522.

McFiggans, G., et al. (2006), The effect of aerosol composition and properties on warm cloud droplet activation, *Atmos. Chem. Phys.*, *6*, 2593–2649.

Mircea, M., et al. (2005), Importance of the organic aerosol fraction for modeling aerosol hygroscopic growth and activation: A case study in the Amazon Basin, *Atmos. Chem. Phys.*, *5*, 3111–3126.

Novakov, T., and C. E. Corrigan (1996), Cloud condensation nucleus activity of the organic component of biomass smoke particles, *Geophys. Res. Lett.*, *23*, 2141–2144.

Novakov, T., C. E. Corrigan, J. E. Penner, C. C. Chuang, O. Rosario, and O. L. Mayol-Bracero (1997), Organic aerosols in the Caribbean trade winds: A natural source?, *J. Geophys. Res.*, *102*, 21,307–21,313.

Rau, J. A. (1989), Composition and size distribution of residential wood smoke particles, *Aerosol Sci. Technol.*, *10*, 181–192.

Reid, J. S., P. V. Hobbs, R. J. Ferek, D. R. Blake, J. V. Martins, M. R. Dunlap, and C. Liousse (1998), Physical, chemical, and optical properties of regional hazes dominated by smoke in Brazil, *J. Geophys. Res.*, *103*, 32,059–32,080.

Ricard, V., J.-L. Jaffrezo, V.-M. Kerminen, R. E. Hillamo, K. Teinilä, and W. Maenhaut (2002), Size distributions and modal parameters of aerosol constituents in northern Finland during the European Arctic Aerosol Study, *J. Geophys. Res.*, *107*(D14), 4208, doi:10.1029/2001JD001130.

Rissler, J., J. Zhou, L. V. Gatti, G. Roberts, M. O. Andreae, and P. Artaxo (2004), Physical properties of the sub-micrometer aerosol over the Amazon rain forest during the wet-to-dry season transition: Comparison of modeled and measured CCN concentrations, *Atmos. Chem. Phys.*, *4*, 2119–2143.

Rissler, J., A. Vestin, E. Swietlicki, G. Fisch, J. Zhou, P. Artaxo, and M. O. Andreae (2006), Size distribution and hygroscopic properties of aerosol particles from dry-season biomass burning in Amazonia, *Atmos. Chem. Phys.*, *6*, 471–491.

Roberts, G. C., P. Artaxo, J. Zhou, E. Swietlicki, and M. O. Andreae (2002), Sensitivity of CCN spectra on chemical and physical properties of aerosol: A case study from the Amazon Basin, *J. Geophys. Res.*, *107*(D20), 8070, doi:10.1029/2001JD000583.

Ruellan, S., H. Cachier, A. Gaudichet, P. Masclet, and J.-P. Lacaux (1999), Airborne aerosols over central Africa during the Experiment for Regional Sources and Sinks of Oxidants (EXPRESSO), *J. Geophys. Res.*, *104*(D23), 30,673–30,690.

Schkolnik, G., A. H. Falkovich, Y. Rudich, W. Maenhaut, and P. Artaxo (2005), A new analytical method for the determination of levoglucosan,

polyhydroxy compounds and 2-methylerythrol and its application to smoke and rainwater samples, *Environ. Sci. Technol.*, *39*, 2744–2752.

Simoneit, B. R. T., J. J. Schauer, C. G. Nolte, D. R. Oros, V. O. Elias, M. P. Fraser, W. F. Rogge, and G. R. Cass (1999), Levoglucosan, a tracer for cellulose in biomass burning and atmospheric particles, *Atmos. Environ.*, *33*, 173–182.

Simoneit, B. R. T., V. O. Elias, M. Kobayashi, K. Kawamura, A. I. Rushdi, P. M. Medeiros, W. F. Rogge, and B. M. Didyk (2004), Sugars: Dominant water-soluble organic components in soils and characterization as tracers in atmospheric particulate matter, *Environ. Sci. Technol.*, *38*, 5939–5949.

Tagliavini, E., F. Moretti, S. Decesari, M. C. Facchini, S. Fuzzi, and W. Maenhaut (2006), Functional group analysis by H NMR/chemical derivatization for the characterization of organic aerosol from the SMOCC field campaign, *Atmos. Chem. Phys.*, *6*, 1003–1019.

Trebs, I., F. X. Meixner, J. Slanina, R. Otjes, P. Jongejan, and M. O. Andreae (2004), Real-time measurements of ammonia, acidic trace gases and water-soluble inorganic aerosol species at a rural site in the Amazon Basin, *Atmos. Chem. Phys.*, *4*, 967–987.

Trebs, I., et al. (2005), The NH_4^+-NO_3^--Cl^--SO_4^{2-}-H_2O aerosol system and its gas phase precursors at a pasture site in the Amazon Basin: How relevant are mineral cations and soluble organic acids?, *J. Geophys. Res.*, *110*, D07303, doi:10.1029/2004JD005478.

Trebs, I., L. L. Lara, L. M. M. Zeri, L. V. Gatti, P. Artaxo, R. Dlugi, J. Slanina, M. O. Andreae, and F. X. Meiner (2006), Dry and wet deposition of inorganic nitrogen compounds to a tropical pasture site (Rondônia, Brazil), *Atmos. Chem. Phys.*, *6*, 447–469.

Wang, W., I. Kourtchev, B. Graham, J. Cafmeyer, W. Maenhaut, and M. Claeys (2005), Characterization of oxygenated derivatives of isoprene related to 2-methyltetrols in Amazonian aerosols using trimethylsilylation and gas chromatography/ion trap mass spectrometry, *Rapid Commun. Mass Spectrom.*, *19*, 1343–1351.

———————————

M. O. Andreae, P. Guyon, A. Hoffer, and I. Trebs, Biogeochemistry Department, Max Planck Institute for Chemistry, D-55020 Mainz, Germany.

P. Artaxo, L. L. Lara, T. Pauliquevis, and L. V. Rizzo, Instituto de Fisica, Universidade de São Paulo, 05508-900 São Paulo, SP, Brazil.

F. Cavalli, S. Decesari, L. Emblico, M. C. Facchini, S. Fuzzi, and M. Mircea, Institute of Atmospheric Sciences and Climate, National Research Council, I-40129 Bologna, Italy. (s.fuzzi@isac.cnr.it; sdecesari@isac.cnr.it)

X. Chi, W. Maenhaut, and N. Raes, Department of Analytical Chemistry, Institute for Nuclear Sciences, Ghent University, BE-9000 Ghent, Belgium.

M. Claeys and I. Kourtchev, Department of Pharmaceutical Sciences, University of Antwerp, BE-2610 Antwerp, Belgium.

A. H. Falkovich, Y. Rudich, and G. Schkolnik, Department of Environmental Sciences, Weizmann Institute, Rehovot 76100, Israel.

G. Fisch, Centro Técnico Aeroespacial, Instituto de Aeronáutica e Espaço, Divisão de Ciências Atmosféricas, 12228-904, São José dos Campos, SP, Brazil.

L. V. Gatti, Divisao de Quimica Ambiental, Instituto de Pesquisas Energéticas e Nucleares, 05508-900 São Paulo, SP, Brazil.

O. L. Mayol-Bracero and L. L. Soto-García, Institute for Tropical Ecosystem Studies, University of Puerto Rico, San Juan, PR 00931-3341, USA.

J. Rissler and E. Swietlicki, Division of Nuclear Physics, Department of Physics, Lund University, S-221 00 Lund, Sweden.

E. Tagliavini, Centro di Ricerche per le Scienze Ambientali, University of Bologna, I-48100 Ravenna, Italy.